haematologica
Journal of the Ferrata Storti Foundation

Targeting P-selectin and interleukin-1β in mice with sickle cell disease: effects on vaso-occlusion, liver injury and organ iron deposition

by Erica M. F. Gotardo, Lidiane S. Torres, Bruna Cunha Zaidan, Lucas F.S. Gushiken, Pamela L. Brito, Flavia C. Leonardo, Claudia H. Pellizzon, John Millholland, Sergei Agoulnik, Jiri Kovarik, Fernando F. Costa, and Nicola Conran

Received: August 14, 2024.
Accepted: November 7, 2024.

Citation: Erica M. F. Gotardo, Lidiane S. Torres, Bruna Cunha Zaidan, Lucas F.S. Gushiken, Pamela L. Brito, Flavia C. Leonardo, Claudia H. Pellizzon, John Millholland, Sergei Agoulnik, Jiri Kovarik, Fernando F. Costa, and Nicola Conran. Targeting P-selectin and interleukin-1 in mice with sickle cell disease: effects on vaso-occlusion, liver injury and organ iron deposition. Haematologica. 2024 Nov 21. doi: 10.3324/haematol.2024.286418 [Epub ahead of print]

Targeting P-selectin and interleukin-1β in mice with sickle cell disease: effects on vaso-occlusion, liver injury and organ iron deposition

Érica M. F. Gotardo[1], Lidiane S. Torres [1,2], Bruna Cunha Zaidan[3], Lucas F. S. Gushiken[1], Pâmela L. Brito[1], Flavia C. Leonardo[1], Claudia H. Pellizzon[4], John Millholland[5*], Sergei Agoulnik[6], Jiri Kovarik[7], Fernando F. Costa[1] and Nicola Conran[1]

[1]Hematology Center, University of Campinas - UNICAMP, Campinas - São Paulo, Brazil;

[2]Ruth L. and David S. Gottesman Institute for Stem Cell and Regenerative Medicine Research, Albert Einstein College of Medicine, Bronx, New York, NY 10461, USA;

[3]Federal University of Triângulo Mineiro, UFTM, Minas Gerais, Brazil;

[4]São Paulo State University (UNESP), Institute of Biosciences, Botucatu, Brazil;

[5]Novartis Precision Medicine, Cambridge, MA, USA;

[6]Novartis Precision Medicine, Cambridge, MA, USA (former affiliation);

[7]Novartis Biomedical Research, Novartis Campus, CH-4056 Basel, Switzerland.

*Currently at Bristol Myers Squibb, Cambridge, MA, USA.

Running title: Targeting P-selectin and IL-1β for sickle cell disease vaso-occlusion and organ injury.

Corresponding author: Nicola Conran, Hematology Center, University of Campinas, Barao Geraldo, Campinas, São Paulo, Brazil. Tel: +55 19 3251 5533. conran@unicamp.br

Acknowledgements

The authors thank Andreas Bruederle, Novartis, Basel, for assistance with study design. We also are grateful to Irene Pereira de Freitas for assistance with flow cytometry and Ana Luisa Bortoluzo de Lorenzo, Hematology Center, UNICAMP, for administrative support. Authors acknowledge FAPESP (the Sao Paulo Research Foundation) and

CAPES (the Coordination for the Improvement of Higher Education Personnel, Brazil) for fellowships awarded to LST, LSFG, and PLB. NC also thanks CNPq (the National Council for Scientific and Technological Development) for research production support.

Author contributions

SA and NC conceived the study. EMFG, SA, LST, JK and NC designed the study. EMFG, LST, LFSG, PLM, and FCL performed experimental work. EMFG, LST, BCZ, CHP, FFC analyzed the data. All authors interpreted the data. EMFG, LST, BCZ, FFC and NC wrote the paper. All authors reviewed and contributed to the final manuscript.

Funding

This study was funded by Novartis Pharma AG. EMFG received funding for a post-doctoral fellowship from Novartis Pharma AG/ FUNCAMP.

Disclosures

NC reports research funding from Novartis Pharma AG. EMFG reports funding of a post-doctoral fellowship from Novartis Pharma AG. JM, SA and JK report current or former employment by Novartis Pharma AG. Authors have no other disclosures relevant to this study to disclose.

Data availability statement

Research datasets for the study are available upon reasonable request from NC.

Abstract

Continuous vaso-occlusive and inflammatory processes cause extensive end-organ damage in adults with sickle cell disease (SCD), and there is little evidence that long-term hydroxyurea therapy prevents this. In initial trials, P-selectin blockade with crizanlizumab reduced SCD vaso-occlusive crisis frequency, and interleukin (IL)-1β inhibition in SCD patients, using canakinumab, lowered inflammatory markers. We used murine SCD models to examine the effects of acute and chronic blockade of P-selectin and of IL-1β on vaso-occlusive events, their inflammatory profile and organ health. Both approaches improved impaired cutaneous microvascular perfusion in SCD mice by reducing TNF-α-induced vaso-occlusion. Acute P-selectin blockade markedly reduced TNF-α-induced neutrophil-platelet aggregate formation in SCD mice, and decreased leukocyte-rolling movements in the microvasculature, while acute IL-1β inhibition attenuated microvascular leukocyte adhesion. Six weeks of IL-1β-blocking immunotherapy improved the inflammatory profile of SCD mice, considerably reduced hepatic fibrosis and provided some relief from lung injury. In contrast, although P-selectin blockade reduced glomerular congestion, no significant benefit to overall organ pathology was observed. Unexpectedly, while combining the two immunotherapies reduced microvascular occlusion, their prolonged use caused acute liver injury. Notably, inhibition of IL-1β, but not of P-selectin, remarkably decreased hemosiderosis, in association with reduced tissue macrophage infiltration and the correction of biomarkers of dysregulated iron turnover. Our findings suggest that the attenuation of inflammation, as well as of vaso-occlusive processes, may be crucial for mitigating organ damage in SCD. Future trials should explore the ability of cytokine blockade to prevent multi-organ damage in patients with SCD, beyond evaluating vaso-occlusive crisis frequency.

Keywords: Adhesion, cytokine, inflammasome, iron, fibrosis, kidney, liver, lung, neutrophils, platelets, vaso-occlusion.

Introduction

Sickle cell disease (SCD), an inherited disorder caused by the production of sickle hemoglobin (HbS),[1] is recognized as an inflammatory disease. SCD clinical complications are numerous, and can be classified as acute (e.g. painful vaso-occlusive crises [VOCs]) or chronic (e.g. kidney disease, hepatopathy) in nature.[2] Characteristic vaso-occlusive processes in SCD arise from altered blood rheology, cellular activation, and adhesive interactions between red blood cells, leukocytes, platelets, and the endothelium. Inflammatory pathways drive the cellular activation that propagates this vaso-occlusion,[3] where amplification of the production of pro-inflammatory cytokines, such as tumor necrosis factor (TNF)-α and interleukin (IL)-1β, promotes endothelial activation and facilitates the cell-cell adhesive interactions that occlude small vessels.[4-6]

Hydroxyurea, presently the most commonly employed disease-modifying therapy in SCD, significantly reduces VOC frequency in SCD patients, with documented improvements in morbidity and mortality.[7] Advances in understanding SCD pathophysiology led to the development of newer therapeutics, such as crizanlizumab, voxelotor and L-glutamine. Crizanlizumab is a humanized monoclonal antibody that binds to P-selectin (CD62P) on the surface of activated endothelial cells and platelets and blocks its interaction with P-selectin glycoprotein ligand-1, predominantly on leukocytes,[8] thereby attenuating cellular recruitment and heterocellular aggregate formation in the vasculature.[9] A phase 2 trial (NCT01895361) demonstrated that crizanlizumab significantly lowered the VOC rate in 198 SCD patients, aged 16 to 65 years, over 52 weeks of treatment,[8] leading to its FDA approval for use in SCD patients aged over 16 years,[10] and later by other agencies. However, the recent STAND study (NCT03814746) failed to confirm the efficiency of crizanlizumab for reducing SCD VOC frequency, compared to placebo, leading to revocation of its authorization in the EU.[11] Inclacumab, another, potentially more potent, P-selectin-blocking molecule is currently under clinical development and in a Phase 3 trial for preventing SCD VOC.[12]

Emerging therapies for SCD have primarily aimed to reduce VOC frequency and/or increase hemoglobin levels. However, advances in the clinical management of SCD have significantly improved the life expectancy of patients, and aging in SCD is worryingly associated with extensive end-organ damage,[13] which is challenging to analyze in clinical trials. Organs affected include the kidneys, brain, liver, heart and

lung, with continuous vaso-occlusion (VO) and inflammatory processes in the vasculature being the most likely causes of such lesions.[3] At this time, there is a dearth of evidence that any of the available disease-modifying agents, including hydroxyurea, can sufficiently prevent end-organ damage in adults with SCD.[14,15] Exploring alternative anti-inflammatory therapeutic strategies to block other inflammatory molecules, or enhancing the benefits of P-selectin blocking therapy by using combination approaches, could further decrease vascular cellular interactions. This may improve VOC onset prevention and, potentially, prevent SCD organ damage.

Canakinumab is a humanized monoclonal antibody that blocks the activity of IL-1β, an inflammasome-processed cytokine that drives inflammatory responses and that is elevated in SCD.[5] A recent randomized, placebo-controlled, multicenter phase 2a study demonstrated that canakinumab was well tolerated in 25 sickle cell anemia (SCA) patients, aged 8 to 20 years, who were treated for 24 weeks.[16] While patients did not report significant reductions in average daily pain, progressive reductions in leukocyte counts and high-sensitivity C-reactive protein were observed, demonstrating the potential anti-inflammatory benefits of IL-1β neutralization. Accordingly, anti-IL1β antibody administration alleviated reperfusion injury, endothelial activation and flow stasis in NY1DD transgenic sickle mice exposed to hypoxia/reoxygenation.[17] Thus, hypothesizing that targeting both adhesive and inflammatory mechanisms could enhance VOC prevention in SCD, we first assessed both the individual and the combined effects of acute P-selectin blockage and IL-1β neutralization on TNF-α-induced VO-like processes in SCD mice. We then looked at the impacts of blocking these pathways, for 6 weeks, on the inflammatory profile and organ injury in SCD mice.

Methods

Antibodies

01BSUR was provided by Novartis BioMedical Research (Basel, Switzerland); RB40.34 and A110-1 IgG1 antibodies were from BD Biosciences (New Jersey, USA).

Animals and treatment protocols

Mice and treatment protocols are detailed in Supplementary Methods. All experimental procedures in animals were approved by the Animal Care and Use Committee of the

University of Campinas (CEUA/ UNICAMP; Protocols 6079-1 and 6179-1), and by Novartis' animal care and use committee.

Intravital microscopy

Observations of the cremaster muscle microcirculation were made in anesthetized SCD mice, as previously described.[18] The microvascular rolling, adhesion and extravasation of leukocytes were quantified. See Supplementary Methods.

Laser Doppler flowmetry

Blood flow and perfusion in the cutaneous microcirculation of the pelvic region of mice was determined as described in Supplementary Methods.

Neutrophil-platelet aggregate quantification

Neutrophil-platelet ($CD45^+Ly6G^+CD41^+$) aggregates were determined in peripheral blood by flow cytometry, as described in Supplementary Material, and calculated using FlowJo V10 software (See Supplementary Figure 1).

Histopathological evaluation

Organs were processed and histological staining/analyses were performed as described in Supplementary Methods.

Quantitative real time-PCR (qPCR)

The extraction of mRNA from organs (stored at -80°C), cDNA synthesis, and the quantitative Real Time PCR protocol are described in Supplementary Materials, as is primer design (Supplementary Table 1).

Statistical analysis

See Supplementary Material.

Results

Acute inhibition of P-selectin and of IL-1β each improve cutaneous microvascular flow and perfusion in TNF-α-challenged SCD mice

Vaso-occlusive processes were induced in male Townes SCD mice by *i.p.* TNF-α administration (Figure 1A). The basal circulating concentrations of IL-1β are elevated in Townes SCD mice, therefore validating use of IL-1β neutralization therapy (Figure 1B). Significant P-selectin-dependent neutrophil-platelet aggregation formation was

observed in the peripheral blood of TNF-α-treated Townes SCD mice, justifying P-selectin blockade use (Figure 1C). Laser Doppler flowmetry demonstrated that administration of TNF-α diminished both blood flow velocity (Figure 1D) and perfusion (Figure 1E) in the hindlimb superficial circulation of Townes SCD mice, compared to basal conditions. Alterations were indicative of the occurrence of VO and reduced tissue blood supply, respectively, in the cutaneous microcirculation.

Anti-CD62P administration (anti-P-selectin; at 30 min before TNF-α, and therefore at 3.5 h before analysis; Figure 1A) restored the TNF-α-induced decrease in cutaneous microvascular blood flow to baseline levels and significantly improved perfusion in mice (Figure 1D and 1E), as did anti-IL-1β administration (21 h before TNF-α, and therefore at 24 h before analysis; Figure 1A). The administration of a combination of both anti-CD62P and anti-IL-1β immunotherapies (30 min and 21 h before TNF-α, respectively) also improved cutaneous blood perfusion in TNF-α-stimulated mice. Of note, the administration of an IgG1 isotype control (mechanistic control for anti-CD62P) slightly, but significantly, increased blood perfusion in TNF-α-induced SCD mice (Figure 1E), but less effectively than P-selectin blockade ($P<0.05$). Previous prolonged-administration studies have shown that the intravenous administration of high dose immunoglobulin (800 mg/kg) can protect mice from neutrophil-mediated vascular injury by blocking FcγRIII,[19] possibly explaining why the low dose of control IgG1 used (approximately 1.2 mg/kg) may slightly improve cutaneous perfusion.

Acute inhibition of P-selectin, but not of IL-1β, abolishes TNF-α-induced heterocellular aggregate formation in SCD mice

Anti-CD62P administration to SCD mice completely abolished the formation of neutrophil-platelet aggregates in TNF-α-stimulated SCD mice (compared to control IgG1 administration), consistent with the known role for P-selectin in the formation of these aggregates (Figure 1C).[20] In contrast, administration of anti-IL-1β antibody did not modulate heterocellular aggregate formation, and combined anti-CD62P and anti-IL-1β administration did not decrease aggregate formation further, compared to anti-CD62P alone.

Acute inhibition of IL-1β potentiates the effects of P-selectin blockade on microvascular TNF-α-induced leukocyte recruitment in SCD mice

Increased leukocyte recruitment in the microvasculature is believed to initiate TNF-α-induced vaso-occlusive processes in SCD mice,[21] thereby reducing blood flow velocity (Figure 1D). TNF-α induced significant leukocyte recruitment in the cremaster microcirculation, increasing leukocyte rolling and adhesion to venule walls (Figure 2A, B). Administration of anti-CD62P abolished TNF-α-induced leukocyte rolling in venues (compared to IgG1; Figure 2A), but did not alter venular leukocyte adhesion (Figure 2B). P-selectin blockade also reduced leukocyte extravasation in the microcirculation (Figure 2C). In contrast, anti-IL-1β administration significantly reduced TNF-α-induced leukocyte adhesion, as well as rolling and extravasation in the SCD mice (compared to saline administration; Fig 2A-D). Importantly, the combination of both anti-CD62P and anti-IL-1β immunotherapies potentiated the inhibition of TNF-α-induced leukocyte recruitment, further decreasing leukocyte rolling and adhesion (compared to anti-IL-1β alone).

TNF-α administration significantly augmented the serum concentrations of the soluble ICAM-1 (sICAM-1) (Figure 2E) and IL-10 (Figure 2F) inflammatory markers. While the abrogating effects of acute P-selectin blockade on circulating sICAM-1 and IL-10 were not significant, acute IL-1β neutralization significantly decreased the TNF-α-induced elevations in serum sICAM-1 and IL-10 in the SCD mice, however combination therapy with the two agents failed to significantly reduce sICAM-1.

Effects of prolonged P-selectin and IL-1β blocking immunotherapies on platelet-leukocyte aggregate formation and the inflammatory profile in Berkeley SCD mice

For prolonged-administration studies, Berkeley mice (4-months old) were treated for 6 weeks with anti-CD62P or anti-IL-1β monotherapies, or their combination. Control animal groups were treated with saline, or an IgG1 control antibody (Figure 3A). Mice were not subjected to TNF-α inflammatory stimulus in these experiments.

Similarly to findings in Townes SCD mice, basal circulating concentrations of IL-1β were significantly elevated in Berkeley mice, compared to C57BL/6 mice (Figure 3B). Likewise, as observed in acute conditions, anti-CD62P immunotherapy significantly reduced neutrophil-platelet aggregate formation in SCD mice, compared to the IgG1 group (Figure 3C), while IL-1β neutralization had no effect. Anti-IL-1β

immunotherapy significantly altered the serum inflammatory profile in SCD mice, decreasing TNF-α (Figure 3D) and IL-6 (Figure 3E) concentrations, but not interferon-γ (Figure 3F). In contrast, anti-CD62P immunotherapy had no significant effect on the levels of inflammatory molecules measured; however, its combination with anti-IL-1β immunotherapy reversed the effect of anti-IL-1β monotherapy on serum IL-6 (Figure 3E).

Effects of prolonged P-selectin and IL-1β blockade on markers of liver and kidney damage in Berkeley SCD mice

Following treatment of Berkeley SCD mice for 6 weeks with saline, IgG1 or immunotherapies, serum biochemical markers of liver damage and of hemolysis were quantified (Supplementary Table 2). Serum alanine aminotransferase (ALT) levels were significantly higher in control saline/IgG1-treated Berkeley mice, compared to untreated age-matched hemizygous (SA) mice, while aspartate aminotransferase (AST) was not significantly altered. Neither monotherapy significantly altered AST or ALT in SCD mice. However, combined anti-CD62P/anti-IL-1β therapy elevated ALT to levels that were significantly higher than those observed for mice that received anti-IL-1β monotherapy.

Total, direct bilirubin, and indirect bilirubin were significantly higher in control saline/IgG1-treated Berkeley SCD mice, compared to hemizygous mice, indicative of accentuated hemolysis and liver dysfunction. A further increase in indirect (unconjugated) bilirubin, in the absence of any alteration in direct bilirubin levels, occurred only in the mice that received the anti-CD62P/anti-IL-1β combination therapy, suggestive of a further increase in hemolysis in these animals.[22] Urine creatinine was significantly lower in IgG1-treated Berkeley SCD mice, compared to aged-matched hemizygous mice, suggestive of renal damage; however, the elevations in urine creatinine observed in the groups treated with anti-CD62P were not statistically significant.

Effects of prolonged P-selectin and IL-1β blockade on hepatic tissue alterations in Berkeley SCD mice

Following the 6-week administration protocols, organs were collected from Berkeley SCD mice euthanatized at 48 hours after the final administration. Histopathological

analysis showed that, compared to aged-matched hemizygotes, the livers of homozygous SCD Berkeley mice treated with saline (or control IgG1) presented vessel and sinusoidal congestion, intralobular necrosis, and pericentral fibrotic bands (Figure 4, H&E; Supplementary Figure 3 highlights histopathological features). Collagen deposition, indicative of fibrosis, was also observed in the liver of saline-treated SCD mice (Figure 4, Masson). Accentuated iron accumulation was also observed, particularly associated with tissue macrophages (Figure 4, Perls; Supplementary Figure 4), together with increased $CD68^+$ cell immunolabelling (Figure 4).

Prolonged anti-CD62P therapy did not significantly alter the congested vessel number or the observations of vessel and sinusoidal congestion in the livers of SCD mice (Figure 4, Figure 6A-B). Furthermore, hepatocyte degeneration and fibrosis were not significantly decreased by anti-CD62P therapy (Figure 6C, E), when compared to IgG1 treatment. Some improvement in sinusoidal/vessel congestion was observed in response to IL-1β neutralization (Figure 4, Figure 6A-B) in SCD mice, when compared to anti-CD62P or saline treatment. This decreased congestion was associated with ameliorations in fibrosis and parameters of acute liver injury (hepatocyte degeneration and lobular necrosis) in the anti-IL1β-treated SCD mice (Figure 4, Figure 6C-E). Combining the anti-CD62P and anti-IL-1β therapies did not potentiate the effects of anti-IL-1β upon vessel congestion and, indeed, appeared to reverse some of this monotherapy's benefits, with increased hepatocyte injury observed (ballooning and steatosis) (Figure 6A-E, Supplementary Figure 3A).

Anti-CD62P therapy had no significant effect on the extensive hepatic iron deposition observed in SCD mice (Figures 4, 6F, 8A). In contrast, and importantly, iron accumulation was almost completely abolished in the livers of mice treated with anti-IL-1β monotherapy, or with the combination of anti-CD62P and anti-IL-1β (Figures 4, 6F, 8A). The presence of $CD68^+$ cells was significantly decreased in mice that received anti-CD62P and/or anti-IL-1β immunotherapies (Figure 4, 6G), although anti-IL-1β monotherapy decreased the macrophage infiltration most effectively.

Effects of prolonged P-selectin and IL-1β blockade on renal and pulmonary tissue alterations in Berkeley SCD mice

Comparing the kidney histopathology of homozygous SCD Berkeley mice treated for 6 weeks with saline, or non-specific IgG1, to that of aged-matched hemizygotes,

glomerular and capillary congestion, and interstitial inflammation with apparent sickled red cells were observed (Figure 5, H&E, and highlighted in Supplementary Figure 3B). Renal collagen deposition close to vessels and the medulla was considered normal in saline/ IgG1-treated SCD mice (Figure 5, Masson), however, iron accumulation was extensive, especially in the proximal tubules, and $CD68^+$ macrophage immunostaining was increased (Figure 5).

Anti-CD62P therapy reduced renal glomerular and capillary congestion, as well as the number of apparent sickled red cells, compared to IgG1-treated SCD mice (Figure 5, 7A-B). In contrast, anti-IL-1β therapy had no significant effect on vessel congestion (Figure 5, Figure 7A-B). Kidney sections from animals receiving combination therapy (anti-CD62P/anti-IL-1β) displayed nephrosclerosis, and glomerular congestion, as well as occasional protein droplet reabsorption, indicating further renal deterioration (Supplementary Figure 3B). Again, anti-IL-1β monotherapy, and its combination with anti-CD62P, completely abolished renal iron deposition in the Berkeley SCD mice (Figure 7D). Notably, $CD68^+$ macrophage infiltration was significantly decreased only in the group treated with anti-IL-1β monotherapy (Figure 5, 7E).

The histopathological observations of the lungs of saline-treated SCD mice indicated alveolar congestion, atelectasis (septal thickening) and some peribronchial inflammation (Supplementary Figures 2 and 3, H&E, Masson), when compared to hemizygote mice. No iron deposition was observed in the lungs of 22-week old SCD mice. While some improvements in the histopathological features of the lungs of SCD mice occurred following the administration of control IgG1 (Supplementary Figure 2, Figure 7G), P-selectin-blocking therapy did not significantly alter SCD lung histopathology. In contrast, Masson staining indicated discrete correction of pulmonary septal thickening in SCD mice that received the anti-IL-1β monotherapy and the combined therapies (Supplementary Figures 2 and 3, Figure 7H).

Effects of prolonged P-selectin and IL-1β blockade on the gene expressions of organ damage markers and iron regulation proteins in Berkeley SCD mice

The gene expressions of tissue damage markers and iron regulation proteins were quantified by qPCR in the organs of SCD mice following treatments (Figure 3A). In SCD mice that received saline, liver expressions of genes encoding collagen type 3,

ICAM-1, TIMP-1, TIMP-2, TGF-β, and HIF-1α were significantly increased compared to hemizygote mice (Supplementary Figure 5A). Immunotherapies targeting P-selectin and IL-1β did not affect the expressions of these genes. In the kidneys, the expression of the gene encoding NGAL, a kidney damage marker, was significantly elevated in saline-treated SCD mice, compared to hemizygotes, while the expression of the KIM-1 gene (*Havcr1*), which has a renal anti-inflammatory role, was unchanged. Immunotherapies did not alter these gene expressions in SCD mouse kidneys (Supplementary Figure 5B).

As significant amelioration of hepatic and renal siderosis was observed in Berkeley SCD mice following anti-IL-1β therapy, we examined the hepatic gene expressions of proteins involved in iron regulation in these mice. In saline-treated SCD mice, the hepatic expressions of genes encoding bone morphogenetic gene-6 (BMP-6) and the transferrin receptor-1 (TrF-1), which mediates iron uptake by cells, were significantly increased compared to age-matched hemizygote controls (Figure 8C-D). After 6 weeks of IL-1β blockade, the expressions of the genes encoding BMP-6 and hepcidin were suppressed in the SCD mouse liver, compared to saline-treated SCD mice (Figure 8B-C).

Discussion

Clinical trials of several disease-modifying therapies in development for SCD have concentrated on assessing VOC frequency and patient-reported pain as primary outcomes.[8,16,23] While reducing VOC frequency in SCD is paramount, there is an urgent need to simultaneously halt irreversible organ damage progression, which significantly impacts morbidity and mortality in patients during adulthood.[24] While early clinical trials in SCD patients showed modest success of P-selectin blocking immunotherapy for decreasing painful VOC,[8] and some reported success for treating SCD priapism,[25,26] its effectiveness for reducing organ damage is less clear. Studies in murine SCD models have shown that blocking P-selectin activity and neutrophil-platelet aggregate formation can resolve pulmonary arteriole microembolisms[9] and inhibit heme-induced acute chest syndrome development.[27] In the acute setting, we found that inhibition of P-selectin inhibited leukocyte rolling, but not adhesion, in the cremaster microcirculation of TNF-challenged Townes SCD mice, in association with inhibition of heterocellular aggregate formation in peripheral blood. Leukocyte rolling is a crucial initial step in the adhesion

and recruitment of leukocytes to the endothelium, and inhibiting these mechanisms restored blood perfusion and flow velocity in the cutaneous microcirculation of these inflamed mice. Conversely, acute P-selectin blockade did not significantly improve the inflammatory profile of these mice. Furthermore, although anti-P-selectin therapy reduced VO processes in SCD mice, 6 weeks of anti-CD62P administration did not modify the inflammatory cytokine profile of Berkeley SCD mice. Notably, while some improvement in renal vessel congestion occurred, hepatocyte degeneration and hepatic injury in these mice were not mitigated by anti-P-selectin therapy. A previous study also reported that P-selectin deficiency in Townes SCD mice did not prevent progressive liver injury.[28]

Acute IL-1β neutralization also successfully restored cutaneous microvascular perfusion and blood flow in TNF-challenged Townes SCD mice. However, unlike the effects of P-selectin inhibition, this improved microvascular blood flow was associated with an inhibition of leukocyte rolling and adhesive interactions, without modulation of heterocellular aggregate formation. Importantly, acute IL-1β neutralization reduced circulating sICAM-1; endothelial ICAM-1 is critical for leukocyte anchoring and typically clusters on TNF-activated endothelium to enhance leukocyte recruitment efficiency.[29] Antibody blockade of IL-1β reduces the endothelial activation induced by CAR-T, tumor cells, and myeloid cells,[30] and it may be postulated that acute IL-1β neutralization restores microvascular blood flow in TNF-challenged SCD mice by blocking endothelial activation. These data suggest that differing mechanistic approaches of inhibition may have similar resulting beneficial effects on occlusion in the microvasculature.

In contrast to the effects of P-selectin blockade, both acute and longer-term IL-1β neutralization ameliorated the inflammatory profile of SCD mice. Prolonged anti-IL-1β administration reduced serum concentrations of TNF-α and IL-6, both major players in molecular inflammatory responses that, along with IL-1β, contribute to liver and renal necrosis and subsequent organ fibrosis.[31-33] Advanced liver injury is implicated in up to 11 % of deaths in individuals with SCD, and severe hepatopathy significantly affects SCD outcome.[34] While depletion of the leukocyte MAC-1 integrin was not previously associated with reduced organ damage in SCD mice,[35] neutralization of IL-1β abrogated hepatic injury in these mice. Anti-IL-1β therapy was also associated with a decrease in septal thickening in the lungs of SCD mice. In contrast, significant renal fibrosis was not apparent in any of the SCD mice at the age studied.

Regarding non-histological biomarkers of organ damage, ALT levels were elevated in SCD Berkeley mice, compared to hemizygote mice, accompanied by an increase in direct bilirubin levels, indicating liver dysfunction and hepatobiliary injury. Although blockade of neither P-selectin nor IL-1β improved these parameters, these data combined with histological observations suggest that, while not reversed, a slowing of organ damage progression occurred. Additionally, although anti-IL-1β therapy tended to improve hepatic ICAM-1 gene expression in SCD mice, no changes occurred in the expressions of genes associated with liver fibrosis or pathology.

Combining the two blocking immunotherapies in the acute protocol reduced microvascular leukocyte recruitment more effectively than either approach alone. This was accompanied by improved cutaneous blood perfusion following TNF challenge and reduced heterocellular aggregate formation. Curiously, the effect of IL-1β neutralization on reducing circulating sICAM-1, suggestive of a beneficial effect on endothelial activation, was abolished when combined with P-selectin inhibition. Furthermore, hepatopathy was exacerbated following prolonged combined immunotherapy, as demonstrated by histological and liver biomarker analysis, and the combination of therapies failed to diminish circulating IL-6. This surprising finding suggests a potential risk for combining these approaches for prolonged use. It is unclear why this hepatopathy occurs during combined therapy; however, the sustained circulation of damaging aged neutrophils,[36] due to their inability to extravasate to sites of inflammation, coupled with continued endothelial activation, may exacerbate hepatic injury.[37] Indeed, processes of sterile inflammation contribute significantly to tissue and organ damage in SCD.[38] A possible role for tissue macrophage accumulation in this hepatotoxicity is further discussed below.

The analyses of organ iron deposition, or hemosiderosis, in SCD mice treated with immunotherapies yielded remarkable findings. Mice treated with saline or the control IgG1 displayed significant and extensive hemosiderosis in the liver sinusoids and renal proximal tubules, with this iron accumulation primarily associated with macrophages. $CD68^+$ immunostaining demonstrated augmented immune cell presence in tissues, where such leukocytes observed in the SCD liver have been previously described as infiltrated monocytes, or macrophages, or resident Küpffer cells.[28] Iron deposition (but not necessarily iron overload) in organs is a characteristic of SCD, even in the absence of regular transfusions,[39,40] and mice models of SCD replicate this condition.[41,42] Such iron accumulation contributes to oxidative stress and inflammation,

particularly in the liver.[43,44] Besides reducing liver fibrosis, 6 weeks of IL-1β neutralization practically eliminated hepatic and renal iron accumulation. Iron quantification confirmed a significant decrease in liver iron content in these mice. Aside iron chelation and iron restriction therapies,[44,45] other therapeutic approaches reported to reduce liver iron deposition in SCD mice have demonstrated relatively discrete improvements.[46,47] The observed effect of IL-1β neutralization on hemosiderosis in SCD mice was associated with the suppression of hepatic gene expressions of hepcidin and BMP-6 (which regulates hepcidin expression). Hepcidin plays a pivotal role in regulating iron metabolism, and our observations are consistent with the correction of iron homeostasis and increased efflux (or downregulated iron uptake) by macrophages and hepatocytes.[48,49]

Although prolonged P-selectin blockade modestly reduced $CD68^+$ cells in the SCD liver, as previously shown after P-selectin deletion in SCD mice,[28] this was not associated with any decrease in organ iron deposition. Decreased macrophage infiltration in the organs of SCD mice treated with anti-IL-1β therapy may be reflective of a reduced necessity to recycle iron. However, while combined anti-CD62P/anti-IL-1β therapy also abolished iron deposition in SCD mice, the presence of renal and hepatic macrophages was greater ($p<0.05$) than in mice subjected to anti-IL-1β monotherapy. It may be that the persistent presence of such macrophages, which are presumably inflammatory in phenotype, in addition to continued endothelial activation and reduced P-selectin-mediated neutrophil recruitment, in the organs of combined therapy-treated SCD mice, contributes to the exacerbated tissue damage in the liver and the sustained inflammatory profile in these mice. Indeed production of IL-6, produced extensively by inflammatory macrophages, was sustained in these mice, as was hepatic hepcidin gene expression, possibly reflective of elevated IL-6.[50]

In conclusion, we investigated the impact of P-selectin and/or IL-1β blockade on vaso-occlusive processes and organ damage in SCD mice, with a summary of findings presented in Supplementary Table 3. While P-selectin blockade successfully reduced microvascular occlusion, restoring blood flow, its effect on organ injury was essentially limited to mitigating vessel congestion. It should be highlighted that no further progression of organ damage occurred during chronic anti-P-selectin monotherapy. IL-1β neutralization reduced vaso-occlusion and decreased hepatic injury by controlling inflammation and reducing organ iron accumulation. Unexpectedly, prolonged combined therapy exacerbated hepatic injury, possibly due to sustained inflammatory

processes and altered macrophage activity, serving as a reminder that combination therapies should be carefully evaluated in preclinical models, and in clinical trials. Our findings emphasize the importance of targeted therapies that simultaneously address both vaso-occlusion and chronic inflammation to improve SCD outcomes. Anti-IL-1β immunotherapy warrants further clinical investigation of its potential to decrease inflammatory and organ damage biomarkers in SCD patients.

References

1. Kato GJ, Piel FB, Reid CD, et al. Sickle cell disease. Nat Rev Dis Primers. 2018;4:18010.
2. Rees DC, Williams TN, Gladwin MT. Sickle-cell disease. Lancet. 2010;376(9757):2018-2031.
3. Conran N, Belcher JD. Inflammation in sickle cell disease. Clin Hemorheol Microcirc. 2018;68(2-3):263-299.
4. Asare K, Gee BE, Stiles JK, et al. Plasma interleukin-1beta concentration is associated with stroke in sickle cell disease. Cytokine. 2010;49(1):39-44.
5. Qari MH, Dier U, Mousa SA. Biomarkers of inflammation, growth factor, and coagulation activation in patients with sickle cell disease. Clin Appl Thromb Hemost. 2012;18(2):195-200.
6. Cerqueira BA, Boas WV, Zanette AD, Reis MG, Goncalves MS. Increased concentrations of IL-18 and uric acid in sickle cell anemia: contribution of hemolysis, endothelial activation and the inflammasome. Cytokine. 2011;56(2):471-476.
7. Steinberg MH, Barton F, Castro O, et al. Effect of hydroxyurea on mortality and morbidity in adult sickle cell anemia: risks and benefits up to 9 years of treatment. JAMA. 2003;289(13):1645-1651.
8. Ataga KI, Kutlar A, Kanter J. Crizanlizumab in Sickle Cell Disease. N Engl J Med. 2017;376(18):1796.
9. Bennewitz MF, Jimenez MA, Vats R, et al. Lung vaso-occlusion in sickle cell disease mediated by arteriolar neutrophil-platelet microemboli. JCI Insight. 2017;2(1):e89761.
10. Karki NR, Kutlar A. P-Selectin Blockade in the Treatment of Painful Vaso-Occlusive Crises in Sickle Cell Disease: A Spotlight on Crizanlizumab. J Pain Res. 2021;14:849-856.
11. Committee for Medicinal Products for Human Use, European Medicines Agency (EMA). Adakveo: Authorisation details (21/8/2023). https://www.ema.europa.eu/en/medicines/human/EPAR/adakveo Accessed on October 25th, 2024.
12. Mayer CL, Koeck K, Hottmann M, et al. A phase 1 study in healthy participants to characterize the safety and pharmacology of inclacumab, a fully human anti-P-selectin antibody, in development for treatment of sickle cell disease. Eur J Clin Pharmacol. 2023;79(9):1219-1228.
13. Vichinsky E. Chronic organ failure in adult sickle cell disease. Hematology Am Soc Hematol Educ Program. 2017;2017(1):435-439.
14. Hankins JS, Ware RE, Rogers ZR, et al. Long-term hydroxyurea therapy for infants with sickle cell anemia: the HUSOFT extension study. Blood. 2005;106(7):2269-2275.
15. Rankine-Mullings AE, Nevitt SJ. Hydroxyurea (hydroxycarbamide) for sickle cell disease. Cochrane Database Syst Rev. 2022;9(9):CD002202.
16. Rees DC, Kilinc Y, Unal S, et al. A randomized, placebo-controlled, double-blind trial of canakinumab in children and young adults with sickle cell anemia. Blood. 2022;139(17):2642-2652.

17. Kaul DK, Thangaswamy S, Suzuka SM, et al. Anti-Interleukin-1 beta Antibody-Based Therapy Ameliorates Endothelial Activation and Inflammation in Sickle Mice. Blood. 2011;118(21):388.
18. Ferreira WA, Jr., Chweih H, Lanaro C, et al. Beneficial Effects of Soluble Guanylyl Cyclase Stimulation and Activation in Sickle Cell Disease Are Amplified by Hydroxyurea: In Vitro and In Vivo Studies. J Pharmacol Exp Ther. 2020;374(3):469-478.
19. Jang JE, Hidalgo A, Frenette PS. Intravenous immunoglobulins modulate neutrophil activation and vascular injury through FcgammaRIII and SHP-1. Circ Res. 2012;110(8):1057-1066.
20. Dominical VM, Samsel L, Nichols JS, et al. Prominent role of platelets in the formation of circulating neutrophil-red cell heterocellular aggregates in sickle cell anemia. Haematologica. 2014;99(11):e214-e217.
21. Turhan A, Weiss LA, Mohandas N, Coller BS, Frenette PS. Primary role for adherent leukocytes in sickle cell vascular occlusion: a new paradigm. Proc Natl Acad Sci U S A. 2002;99(5):3047-3051.
22. Doig K. Introduction to increased destruction of erythrocytes. In: Keohane KH, Otto CN, Walenga JM, eds. Rodak's Hematology: Clinical Principles and Applications. Sixth Edition ed: Elsevier Inc. , 2020:316-335.
23. Niihara Y, Smith WR, Stark CW. A Phase 3 Trial of l-Glutamine in Sickle Cell Disease. N Engl J Med. 2018;379(19):226-235.
24. Sharpe CC, Suddle A, Stuart-Smith S. An Overview of Solid Organ Transplantation in Patients With Sickle Cell Disease. Transplantation. 2023;107(3):596-604.
25. Idowu M, DeBaun MR, Burnett A, et al. Primary Analysis of Spartan: A Phase 2 Trial to Assess the Efficacy and Safety of Crizanlizumab in Patients with Sickle Cell Disease Related Priapism. Blood. 2023;142(Supplement 1):146.
26. Idowu M, Garcia RL, Sule OB. Successful Treatment of SCD-Related Priapism With Crizanlizumab: A Case Series. J Investig Med High Impact Case Rep. 2023;11:23247096231191873.
27. Ghosh S, Flage B, Weidert F, Ofori-Acquah SF. P-selectin plays a role in haem-induced acute lung injury in sickle mice. Br J Haematol. 2019;186(2):329-333.
28. Vats R, Kaminski TW, Ju EM, et al. P-selectin deficiency promotes liver senescence in sickle cell disease mice. Blood. 2021;137(19):2676-2680.
29. van Buul JD, van Rijssel J, van Alphen FP, et al. Inside-out regulation of ICAM-1 dynamics in TNF-alpha-activated endothelium. PLoS One. 2010;5(6):e11336.
30. Chen Y, Li R, Shang S, et al. Therapeutic Potential of TNFalpha and IL1beta Blockade for CRS/ICANS in CAR-T Therapy via Ameliorating Endothelial Activation. Front Immunol. 2021;12:623610.
31. Pratim Das P, Medhi S. Role of inflammasomes and cytokines in immune dysfunction of liver cirrhosis. Cytokine. 2023;170:156347.
32. Chen H, Yang Y, Zhou X, Feng Y. Attenuating Renal Interstitial Fibrosis by Shenqi Pill via Reducing Inflammation Response Regulated by NF-kappaB Pathway In Vitro and In Vivo. Iran J Kidney Dis. 2024;18(2):87-98.
33. Duan X, Chen C, Liu X, et al. Interference of periostin attenuates pathological changes, proinflammatory markers and renal fibrosis in diabetic kidney injury. Genes Genomics. 2023;45(11):1389-1397.
34. Duvoux C, Blaise L, Matimbo JJ, et al. The liver in sickle cell disease. Presse Med. 2023;52(4):104212.
35. Chen G, Chang J, Zhang D, et al. Targeting Mac-1-mediated leukocyte-RBC interactions uncouples the benefits for acute vaso-occlusion and chronic organ damage. Exp Hematol. 2016;44(10):940-946.
36. Zhang D, Chen G, Manwani D, et al. Neutrophil ageing is regulated by the microbiome. Nature. 2015;525(7570):528-532.
37. Shi J, Fujieda H, Kokubo Y, Wake K. Apoptosis of neutrophils and their elimination by Kupffer cells in rat liver. Hepatology. 1996;24(5):1256-1263.

38. Rarick KR, Li K, Teng RJ, et al. Sterile inflammation induces vasculopathy and chronic lung injury in murine sickle cell disease. Free Radic Biol Med. 2024;215:112-126.
39. Voskaridou E, Douskou M, Terpos E, et al. Magnetic resonance imaging in the evaluation of iron overload in patients with beta thalassaemia and sickle cell disease. Br J Haematol. 2004;126(5):736-742.
40. Yassin M, Soliman A, De Sanctis V, et al. Liver Iron Content (LIC) in Adults with Sickle Cell Disease (SCD): Correlation with Serum Ferritin and Liver Enzymes Concentrations in Transfusion Dependent (TD-SCD) and Non-Transfusion Dependent (NT-SCD) Patients. Mediterr J Hematol Infect Dis. 2017;9(1):e2017037.
41. Manci EA, Hillery CA, Bodian CA, et al. Pathology of Berkeley sickle cell mice: similarities and differences with human sickle cell disease. Blood. 2006;107(4):1651-1658.
42. Williams JD, Kumar R, Afolabi JM, Park F, Adebiyi A. Rhabdomyolysis aggravates renal iron accumulation and acute kidney injury in a humanized mouse model of sickle cell disease. Free Radic Res. 2023;57(6-12):404-412.
43. Kaminski TW, Sivanantham A, Mozhenkova A, et al. Hemoglobin scavenger receptor CD163 as a potential biomarker of hemolysis induced hepatobiliary injury in sickle cell disease. Am J Physiol Cell Physiol. 2024;327(2):C423-C437.
44. Li H, Kazmi JS, Lee S, et al. Dietary iron restriction protects against vaso-occlusion and organ damage in murine sickle cell disease. Blood. 2023;141(2):194-199.
45. Hamdy M, El-Beshlawy A, Verissimo MPA, et al. Deferiprone versus deferoxamine for transfusional iron overload in sickle cell disease and other anemias: Pediatric subgroup analysis of the randomized, open-label FIRST study. Pediatr Blood Cancer. 2024;71(1):e30711.
46. Katoch O, Ungalara R, Kaminski T, et al. Long-Term L-Glutamine Treatment Reduces Hemolysis without Ameliorating Hepatic Vaso-Occlusion and Liver Fibrosis in a Mouse Model of Sickle Cell Disease. Biomedicines. 2023;11(9):2412.
47. Federti E, Matte A, Recchiuti A, et al. In Humanized Sickle Cell Mice, Imatinib Protects Against Sickle Cell-Related Injury. Hemasphere. 2023;7(3):e848.
48. Afsar RE, Kanbay M, Ibis A, Afsar B. In-depth review: is hepcidin a marker for the heart and the kidney? Mol Cell Biochem. 2021;476(9):3365-3381.
49. Zheng H, Yang F, Deng K, et al. Relationship between iron overload caused by abnormal hepcidin expression and liver disease: A review. Medicine (Baltimore). 2023;102(11):e33225.
50. Kowdley KV, Gochanour EM, Sundaram V, Shah RA, Handa P. Hepcidin Signaling in Health and Disease: Ironing Out the Details. Hepatol Commun. 2021;5(5):723-735.

Legends to Figures

Figure 1. Acute P-selectin blockade and IL-1β neutralization in mice with sickle cell disease (SCD) reverse TNF-α cytokine-induced cutaneous microvascular dysfunction, in association with differing effects on heterocellular aggregation formation. (A) Experimental design for acute protocols in SCD mice. Townes SCD mice were treated intraperitoneally (i.p.) with antibodies targeting P-selectin (anti-CD62P) and/or IL-1β (anti-IL-1β), at 3.5 h or 24 h (respectively) prior to analysis, consisting of laser Doppler flowmetry of the skin, blood sampling or intravital microscopy. Mice were also subjected to Laser Doppler flowmetry at 48 h before protocols to measure basal hemodynamics. Doses were administered as follows: Saline (100μL, 24 h before analysis, n=5 or 6); 30 μg/mouse IgG1 isotype control antibody (A110-1, 3.5 h before analysis, n=6); 30 μg/mouse anti-CD62P (RB40.34, 3.5 h before analysis, n=5/ 6); 200 μg/mouse anti-IL-1β (01BSUR, 24h before analysis, n=5/6), and 30 μg/mouse anti-CD62P plus 200 μg/mouse anti-IL-1β (n=6). Inflammatory processes were induced in mice by the administration of TNF-α (TNF) at 3 h before flowmetry/ blood sampling/ intravital microscopy (0.5μg, *i.p.*). **(B)** Basal levels of IL-1β were measured in the serum of C57BL/6J mice (C57, n=10) and Townes SCD mice (Tow, n=13) by ELISA. **(C)** Flow cytometry was used to monitor neutrophil-platelet heterocellular aggregate formation in the blood of SCD mice. Platelet-neutrophil aggregates were determined as the percentage of $CD45^{+}Ly6G^{+}$ neutrophils in peripheral blood samples of mice that also labelled positive for the platelet marker, CD41. Laser Doppler flowmetry (PeriFlux 6000; Perimed) was used to measure blood flow **(D)** and perfusion **(E)** in the hindlimb superficial microcirculation of SCD mice. Data were normalized relative to basal measurements taken from the same mice, 48 h earlier. B-E, statistical comparisons are made between treatments and their mechanistic control, and between treatments.

Figure 2. Acute P-selectin blockade and IL-1β neutralization modulate TNFα-induced leukocyte recruitment and vaso-occlusive-like processes in mice with sickle cell disease (SCD). Townes SCD mice were treated i.p. with antibodies targeting P-selectin (anti-CD62P) and/or the inflammasome-processed cytokine, IL-1β (anti-IL-1β), at 3.5 or 24h, respectively, prior to intravital microscopy (n= 5-6 per group)(See Figure 1A). Vaso-occlusive processes were induced in mice by the administration of TNF-α (TNF, 0.5μg, *i.p.*): Leukocyte (WBC) recruitment was quantified in 5-9 venules of the cremaster muscle of each mouse at 180 min after TNF. Graphs depict WBC rolling along the venule walls (100 μm) **(A)**, WBC adhesion **(B),** and WBC extravasation **(C)**. Circles represent values for each venule. **(D)** Representative photomicrographs from a cremaster venule in each treatment group; bars represent 20 μm. Note the visible improvement in venular blood flow in animals treated with anti-CD62P, anti-IL-1β, or their combination, compared to the venules of TNF-challenged mice (and IgG1/TNF-treated mice), where individual cells (indicated by *) can be distinctly observed, indicating vaso-occlusion. White arrows indicate the direction of blood flow. Serum concentrations of **(E)** soluble ICAM-1 (sICAM-1), and **(F)** IL-10 were determined by ELISA. A-C and E-F, statistical comparisons are made between treatments and their mechanistic control, and between treatments.

Figure 3. Anti-inflammatory effects of chronic administration (six weeks) of immunotherapies that block P-selectin and/or IL-1β in sickle cell disease (SCD) mice. (A) Experimental design: Berkeley mice (4-months old) were treated with *i.p.* injections of 30 μg/ mouse anti-CD62P (n=9-10) or equivalent IgG1 (n=9), three times a

week, and /or 7.5 mg/Kg of anti-IL1β antibody (n=7-9) or saline (n=10), twice a week, for 6 weeks. At 48 h after administration of the final intervention dose, peripheral blood samples and organs of mice were collected and appropriately stored for processing. **(B)** Basal levels of IL-1β were measured in the serum of C57BL/6J mice (C57, n=10) and Berkeley SCD mice (Berk, n=7) by ELISA. **(C)** Platelet-neutrophil aggregates were monitored in peripheral blood samples by flow cytometry, and serum concentrations of **(D)** TNF-α, **(E)** IL-6 and **(F)** IFN-γ were determined by ELISA. Platelet-neutrophil aggregates are expressed as the percentage of neutrophils (CD45+/Ly6G+) that also displayed labeling for the platelet marker, CD41. C-F, statistical comparisons are made between treatments and their mechanistic control, and between treatments.

Figure 4. Effects of 6-weeks administration of anti-CD62P and anti-IL-1β immunotherapies on liver histology, injury, and iron accumulation in sickle cell disease (SCD) mice. Berkeley SCD mice (4-months old) were treated with immunotherapies, or not, as described in Figure 3A, for 6 weeks. At 48 h after administration of the final intervention dose, livers were dissected and processed for histological analysis (H & E staining, 20 x magnification), analysis of fibrosis (Masson Trichrome, 20x mag.), iron accumulation (Perls Prussian blue, 63x mag.), and $CD68^+$ cells (anti-CD68 immunohistochemical staining, 20x mag.). Image depicts representative photographs of stained sections from each treatment group and comparison with liver sections from hemizygous Berkeley control mice of the same age. Photographs are representative of four images per section (2-4 sections per mouse). Black arrows: congested vessels; yellow arrows: collagen deposits; yellow circles: areas of macrophage infiltration. Photomicrographs taken with a Zeiss Axio Imager D2.

Figure 5. Effects of 6-weeks administration of anti-CD62P and anti-IL-1β immunotherapies on kidney histology, injury, and iron accumulation in sickle cell disease (SCD) mice. Berkeley SCD mice (4-months old) were treated, or not, with immunotherapies, as described in Figure 3A, for 6 weeks. At 48 h after administration of the final intervention dose, kidneys were dissected and processed for histological analysis (H & E staining, 20 x magnification), analysis of fibrosis (Masson Trichrome, 20x mag.), iron accumulation (Perls Prussian blue, 63x mag.), and $CD68^+$ cell infiltration (anti-CD68 immunohistochemical staining, 20x mag.). Image depicts representative photographs of stained sections from each treatment group and comparison with kidney sections from hemizygous Berkeley control mice of the same age. Photographs are representative of four images per section (2-4 sections per mouse). Black arrows: congested vessels; yellow arrows: collagen deposits; yellow circles: areas of macrophage infiltration. Photomicrographs taken with a Zeiss Axio Imager D2.

Figure 6. Morphometric analysis, histopathological evaluation and quantification of collagen, iron and macrophage infiltration in the livers of Berkeley sickle cell disease (SCD) mice after 6 weeks of immunotherapies. Berkeley SCD mice (4-months old) were treated, or not, with immunotherapies, as described in Figure 3A, for 6 weeks. At 48 h after administration of the final intervention dose, livers were dissected and processed for analysis in 2-4 histological slices per animal (n=4/ group). The following analyses were performed in H & E stained sections: (A) Morphometric analysis of the number of congested vessels (count μm^{-2}); (B) congestion in sinusoids and vessels; (C) hepatic degradation score; (D) centrilobular necrosis score. (E) Analysis of collagen fiber deposition (Masson Trichrome; AU staining intensity μm^{-2}). (F) Hemosiderin quantification (Perls staining; staining intensity μm^{-2}), and

quantification of (G) monocyte/macrophage infiltration (anti-CD68 immunohistochemical staining; AU of staining intensity μm^{-2}).

Figure 7. Histopathological evaluation and quantification of collagen, iron and macrophage infiltration in the kidneys and lungs of Berkeley sickle cell disease (SCD) mice after 6 weeks of immunotherapies. Berkeley SCD mice (4-months old) were treated, or not, with immunotherapies, as described in Figure 3A, for 6 weeks. At 48 h after administration of the final intervention dose, kidneys, and lungs were dissected and processed for analysis in 2-4 histological slices per animal (n=4/ group). Kidneys: (A) congestion in glomerular vessels and capillaries; (B) red blood cell (RBC) sickling score. (C) Analysis of collagen fiber deposition (Masson Trichrome; AU staining intensity μm^{-2}). (D) Hemosiderin quantification (Perls; staining intensity μm^{-2}). (E) Analysis of monocyte/ macrophage infiltration (anti-CD68 immunohistochemical staining; AU of staining intensity μm^{-2}). Lungs, H&E staining: (F) Congestion in alveolar vessels; (G) septal thickening score. (H) Analysis of collagen fiber deposition, mainly in the interalveolar septa (Masson Trichrome; AU staining intensity μm^{-2}). Statistical comparisons are made between treatments and their mechanistic control, and between treatments.

Figure 8. Effects of 6-weeks administration of anti-CD62P and anti-IL-1β immunotherapies on liver iron content and the gene expression of markers of iron regulation in livers from sickle cell disease (SCD) mice. Berkeley SCD mice (4-months old) were treated, or not, with immunotherapies, as described in Figure 3A, for 6 weeks. At 48 h after administration of the final intervention dose, livers were dissected and processed for iron measurement and analysis of gene expression by quantitative PCR. (A) Total and free iron in liver homogenates (nMols/mg tissue). (B-D) Organs from aged-matched hemizygous littermate mice (Hemi) were used for histopathological comparisons. Expressions of the genes encoding (B) hepcidin (*Hamp*), (C) bone morphogenetic protein-6 (BMP-6, *Bmp6*) and (D) transferrin receptor-1 (TrF-1, *Tfrc*) were normalized to the expression of *Actb* and *Gapdh*. Statistical comparisons are made between treatments and their mechanistic control, and between treatments.

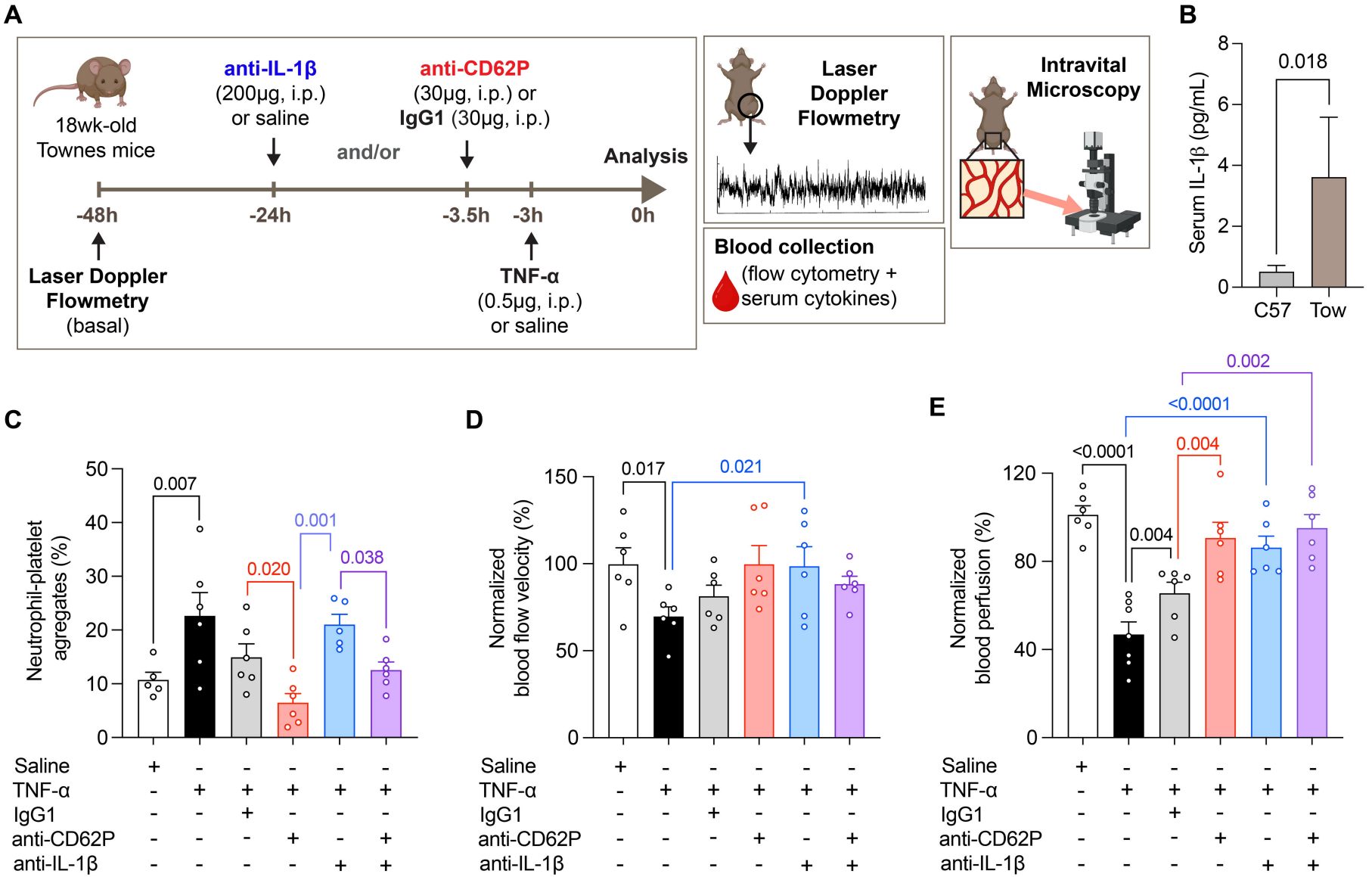
A
18wk-old
Townes mice
anti-IL-1β
(200µg, i.p.)
or saline
anti-CD62P
(30µg, i.p.) or
IgG1 (30µg, i.p.)
and/or
Analysis
-48h
-24h
-3.5h
-3h
0h
Laser Doppler
Flowmetry
(basal)
TNF-α
(0.5µg, i.p.)
or saline
Laser
Doppler
Flowmetry
Intravital
Microscopy
Blood collection
(flow cytometry +
serum cytokines)
B
Serum IL-1β (pg/mL)
0.018
C57
Tow
C
Neutrophil-platelet
agregates (%)
0.007
0.020
0.001
0.038
D
Normalized
blood flow velocity (%)
0.017
0.021
E
Normalized
blood perfusion (%)
<0.0001
0.004
<0.0001
0.004
0.002
Saline
TNF-α
IgG1
anti-CD62P
anti-IL-1β

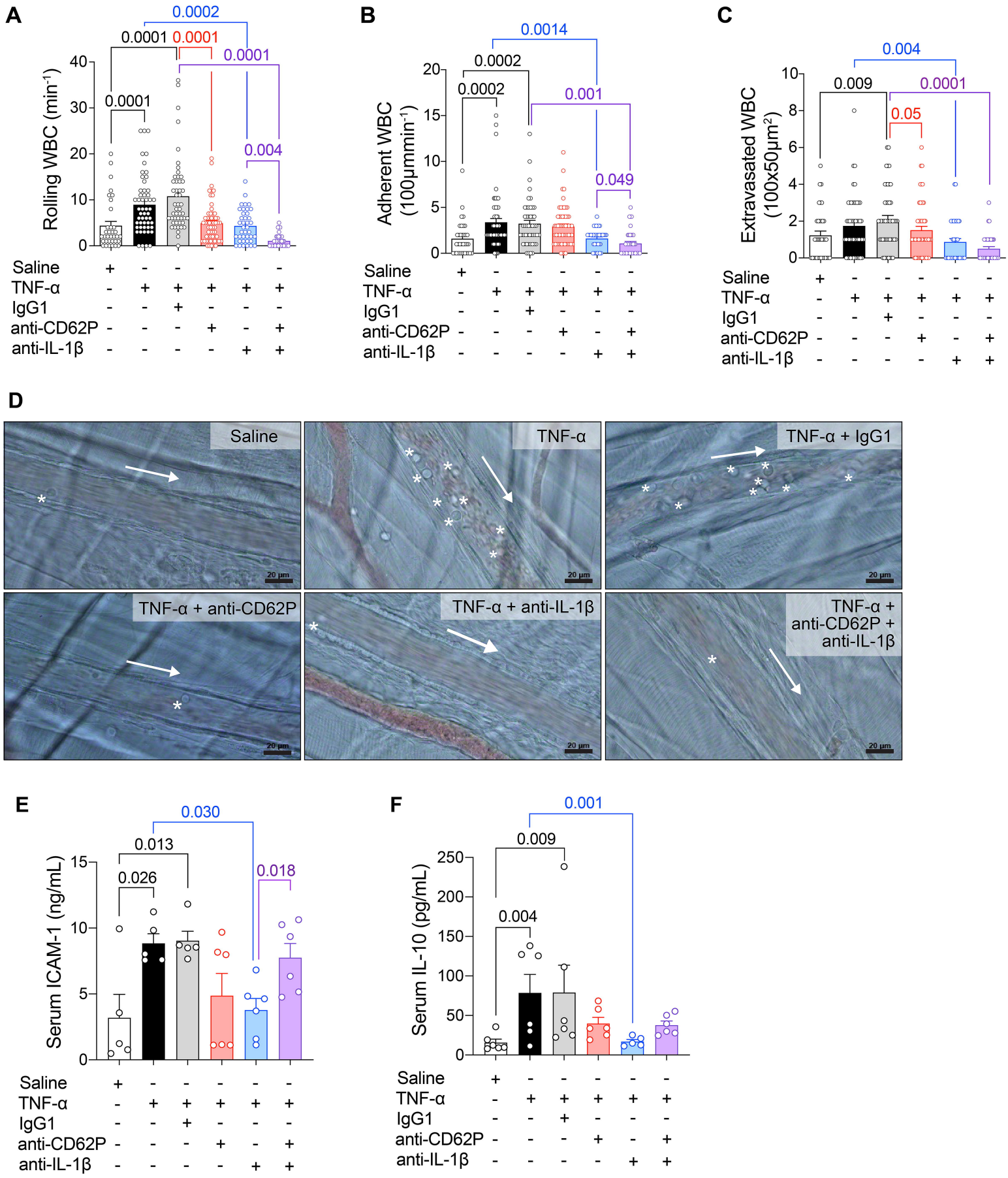
A
Rolling WBC (min-1)
0.0002
0.0001
0.0001
0.0001
0.0001
0.004
B
Adherent WBC (100µmmin-1)
0.0014
0.0002
0.0002
0.001
0.049
C
Extravasated WBC (100x50µm2)
0.004
0.009
0.0001
0.05
Saline
TNF-α
IgG1
anti-CD62P
anti-IL-1β
D
Saline
TNF-α
TNF-α + IgG1
TNF-α + anti-CD62P
TNF-α + anti-IL-1β
TNF-α + anti-CD62P + anti-IL-1β
20 µm
E
Serum ICAM-1 (ng/mL)
0.030
0.013
0.026
0.018
F
Serum IL-10 (pg/mL)
0.001
0.009
0.004

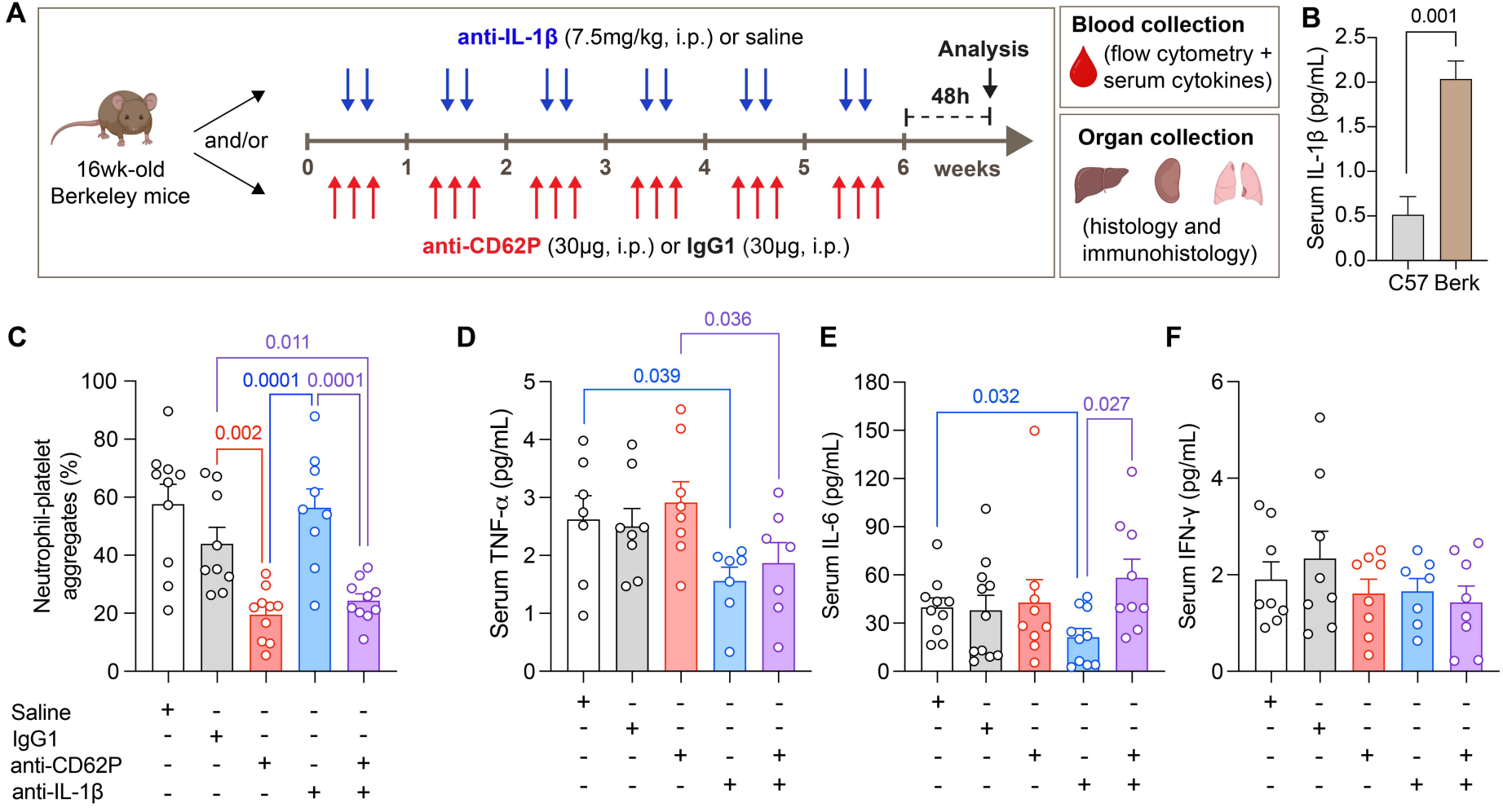
A
anti-IL-1β (7.5mg/kg, i.p.) or saline
Analysis
48h
16wk-old
Berkeley mice
and/or
0
1
2
3
4
5
6
weeks
anti-CD62P (30μg, i.p.) or IgG1 (30μg, i.p.)
Blood collection
(flow cytometry +
serum cytokines)
Organ collection
(histology and
immunohistology)
B
0.001
Serum IL-1β (pg/mL)
2.5
2.0
1.5
1.0
0.5
0.0
C57 Berk
C
0.011
0.0001
0.0001
0.002
Neutrophil-platelet
aggregates (%)
100
80
60
40
20
0
Saline
IgG1
anti-CD62P
anti-IL-1β
D
0.036
0.039
Serum TNF-α (pg/mL)
5
4
3
2
1
0
E
0.032
0.027
Serum IL-6 (pg/mL)
180
150
120
90
60
30
0
F
Serum IFN-γ (pg/mL)
6
4
2
0

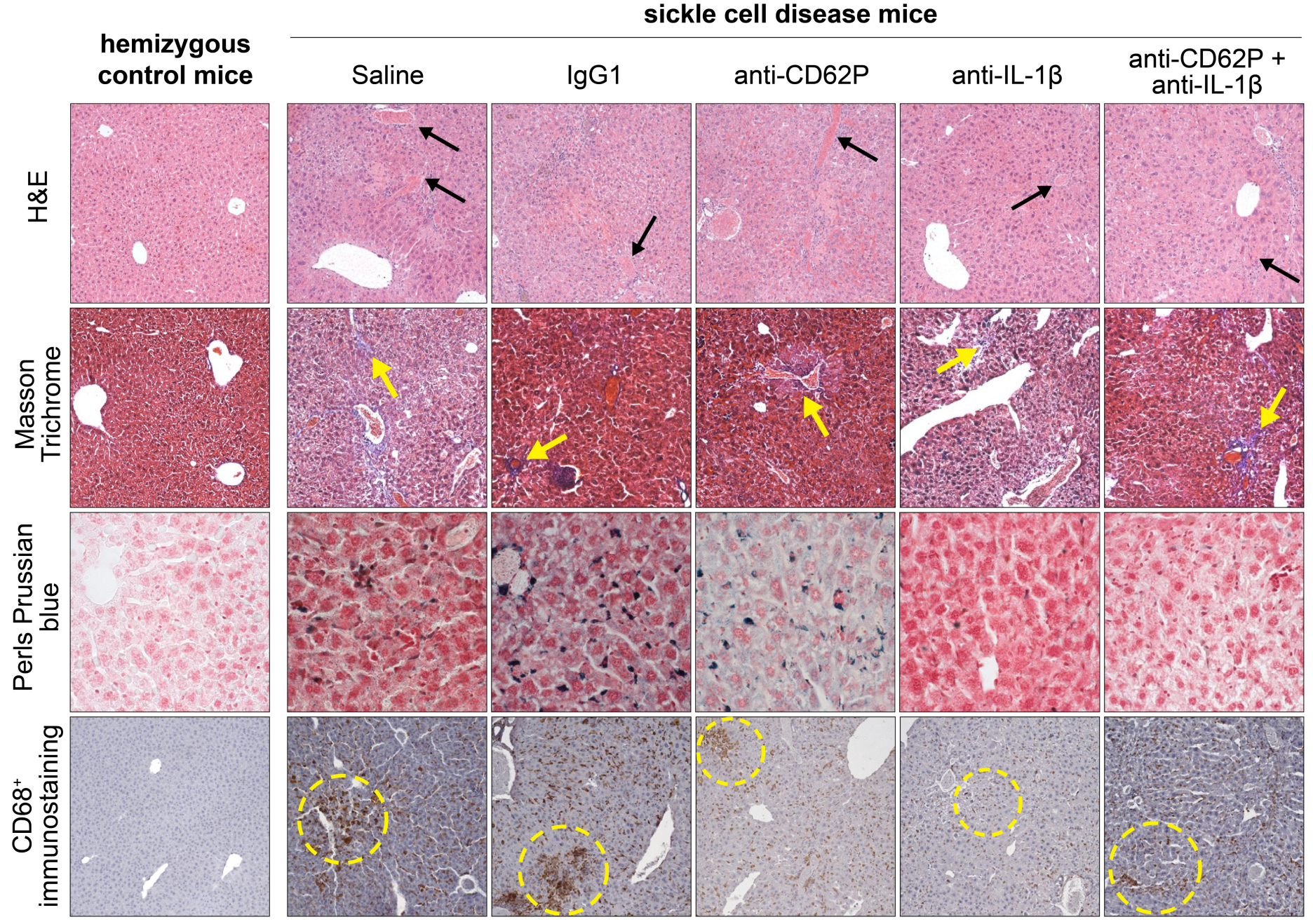
sickle cell disease mice
hemizygous control mice
Saline
IgG1
anti-CD62P
anti-IL-1β
anti-CD62P + anti-IL-1β
H&E
Masson Trichrome
Perls Prussian blue
CD68+ immunostaining

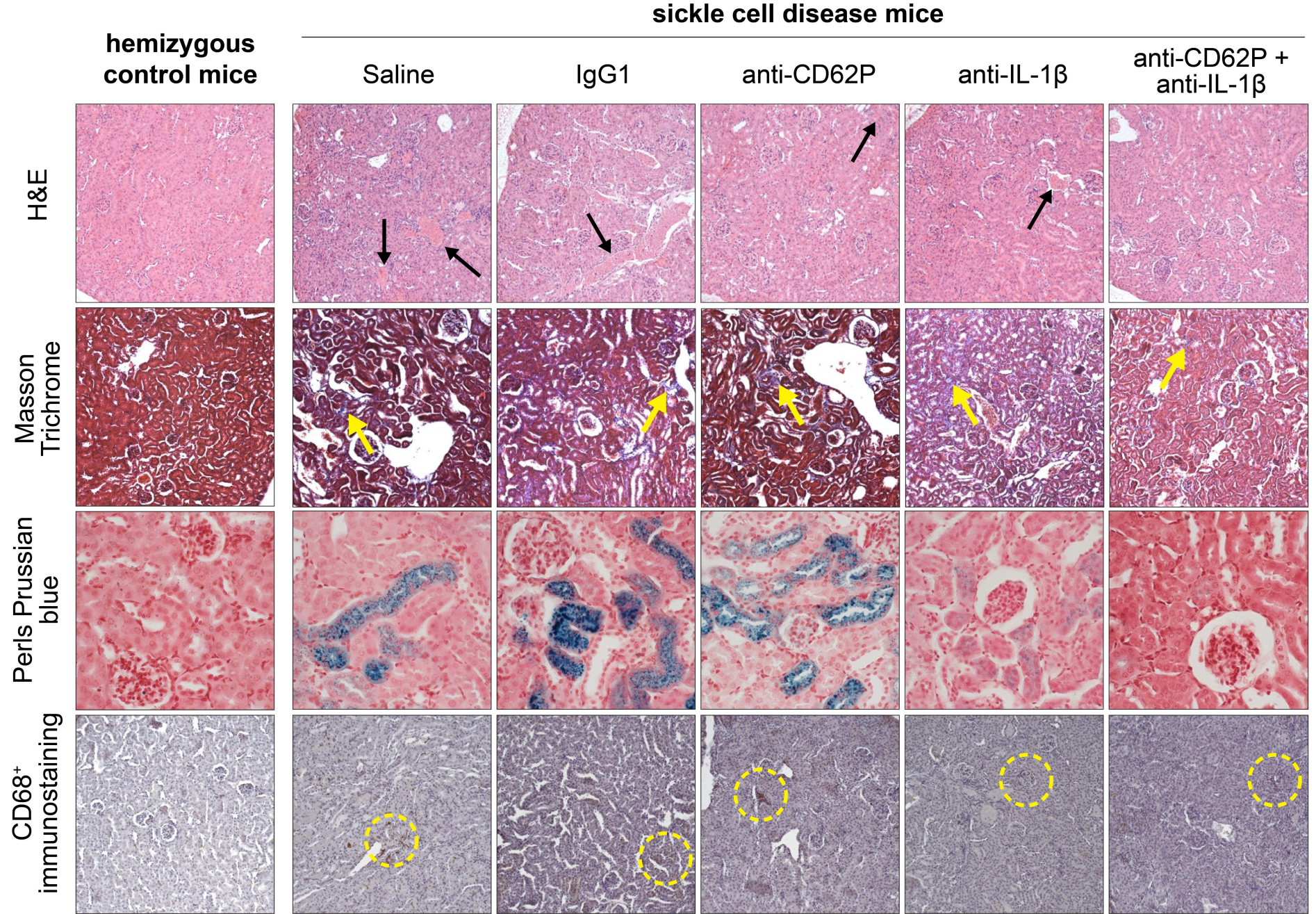
sickle cell disease mice
hemizygous control mice
Saline
IgG1
anti-CD62P
anti-IL-1β
anti-CD62P + anti-IL-1β
H&E
Masson Trichrome
Perls Prussian blue
CD68+ immunostaining

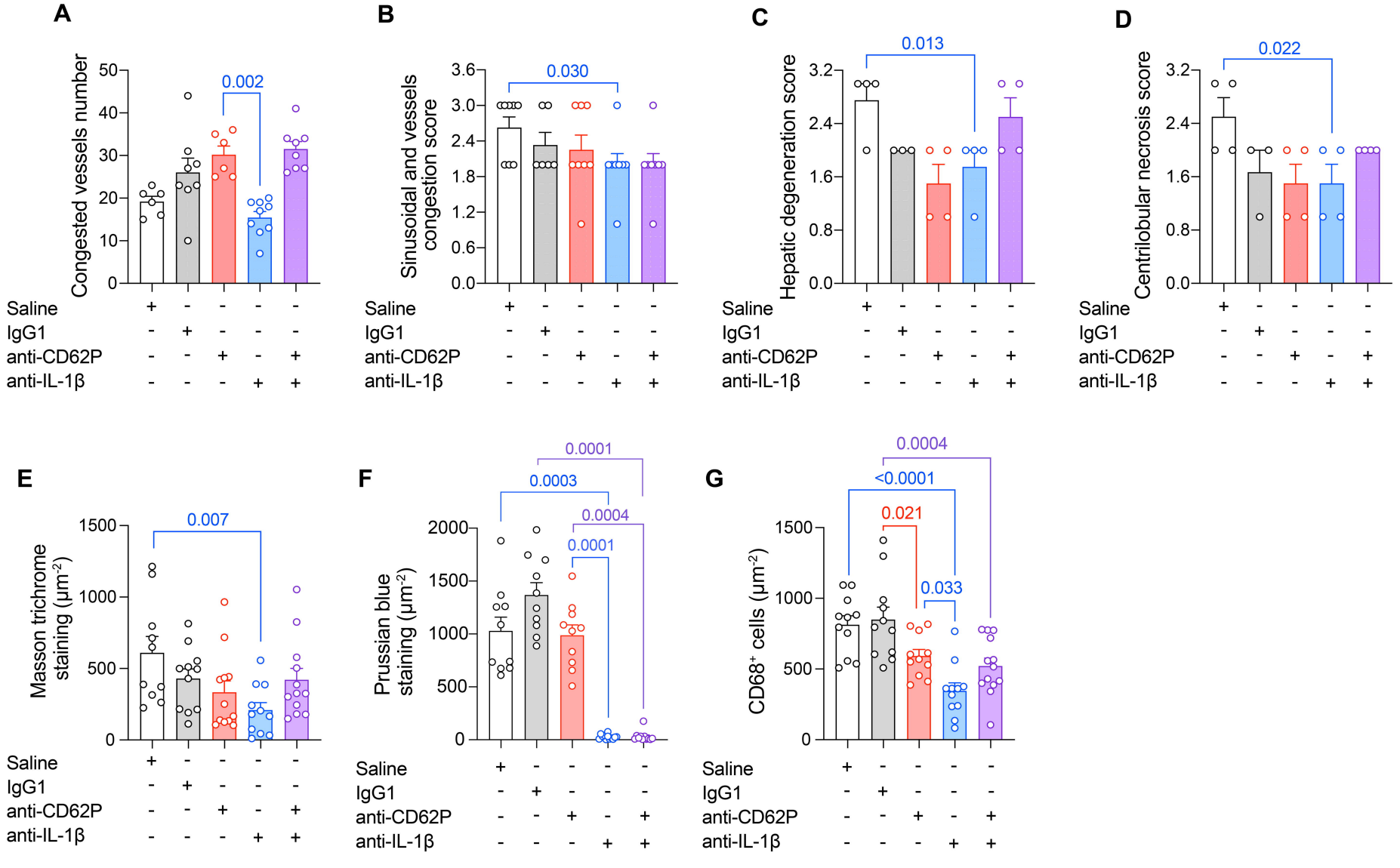
A
Congested vessels number
0.002
B
Sinusoidal and vessels congestion score
0.030
C
Hepatic degeneration score
0.013
D
Centrilobular necrosis score
0.022
E
Masson trichrome staining (µm-2)
0.007
F
Prussian blue staining (µm-2)
0.0001
0.0003
0.0004
0.0001
G
CD68+ cells (µm-2)
0.0004
<0.0001
0.021
0.033
Saline
IgG1
anti-CD62P
anti-IL-1β

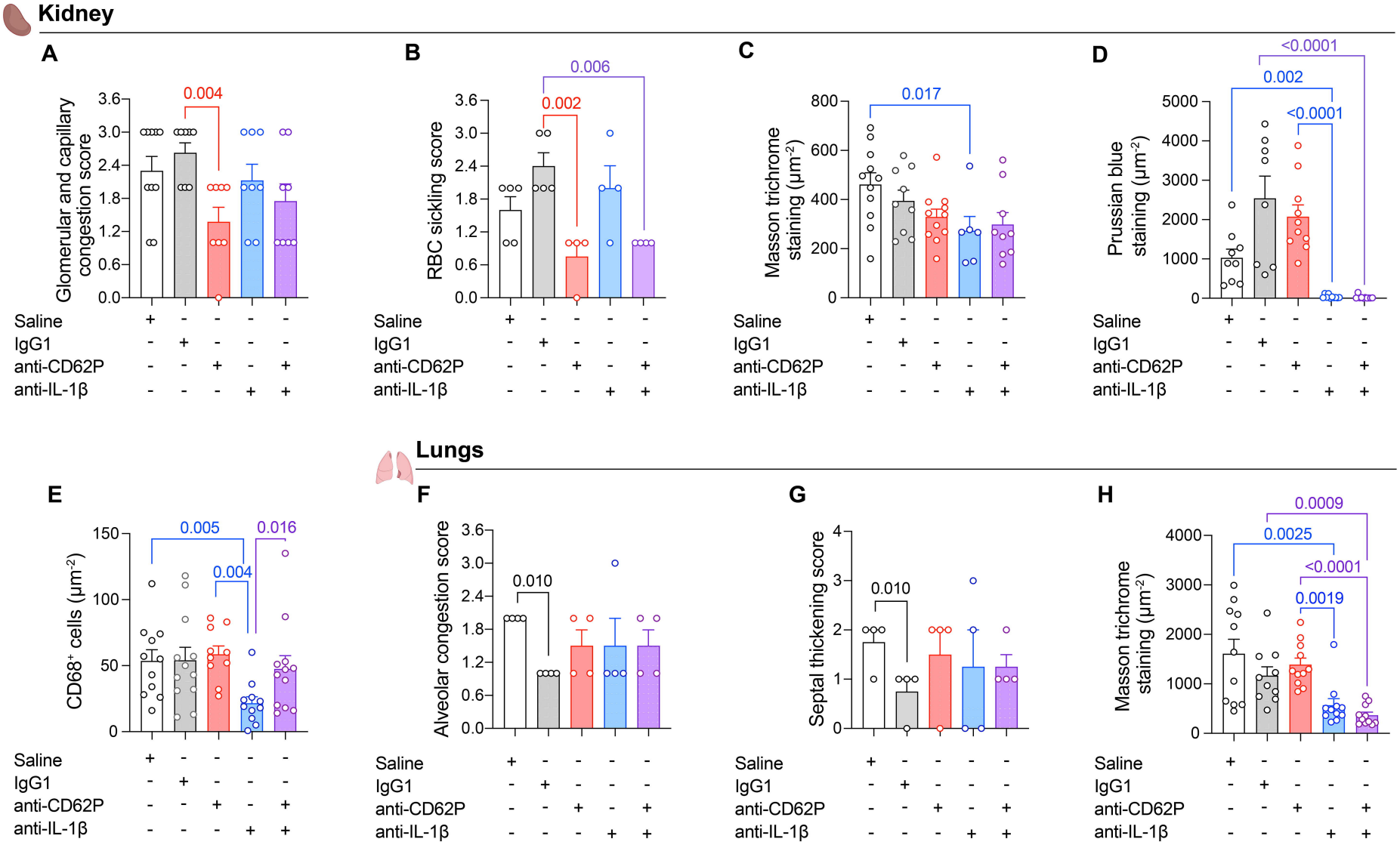
Kidney
A
Glomerular and capillary congestion score
0.004
B
RBC sickling score
0.006
0.002
C
Masson trichrome staining (µm-2)
0.017
D
Prussian blue staining (µm-2)
<0.0001
0.002
<0.0001
Saline
IgG1
anti-CD62P
anti-IL-1β
Lungs
E
CD68+ cells (µm-2)
0.005
0.016
0.004
F
Alveolar congestion score
0.010
G
Septal thickening score
0.010
H
Masson trichrome staining (µm-2)
0.0009
0.0025
<0.0001
0.0019

Liver

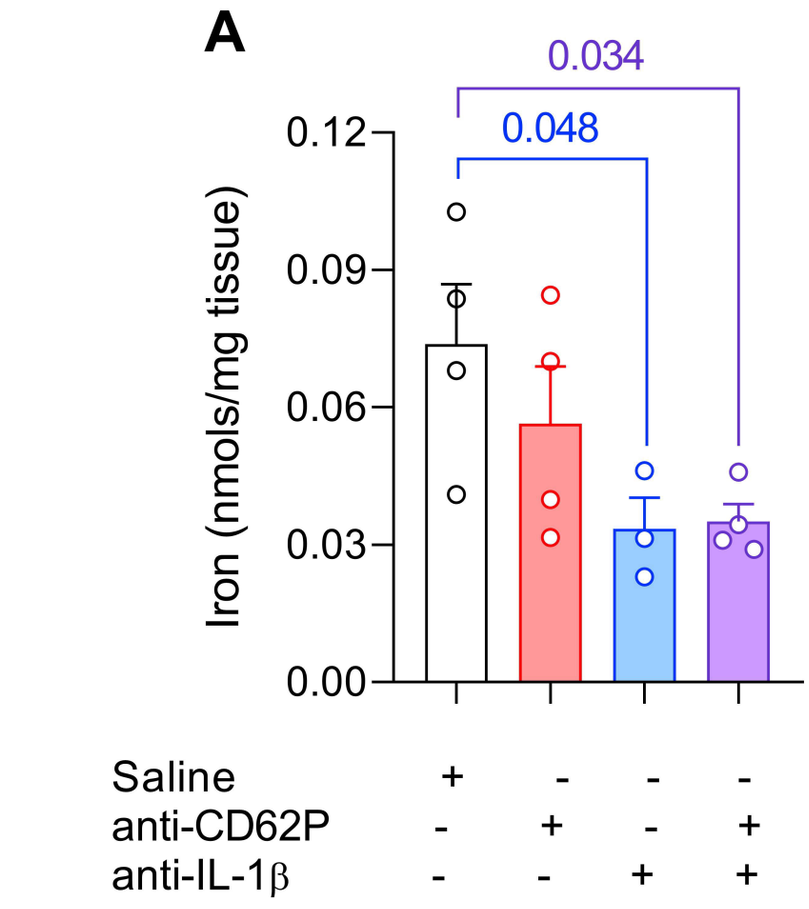
A
0.034
0.048
0.12
0.09
0.06
0.03
0.00
Iron (nmols/mg tissue)
Saline + - - -
anti-CD62P - + - +
anti-IL-1β - - + +

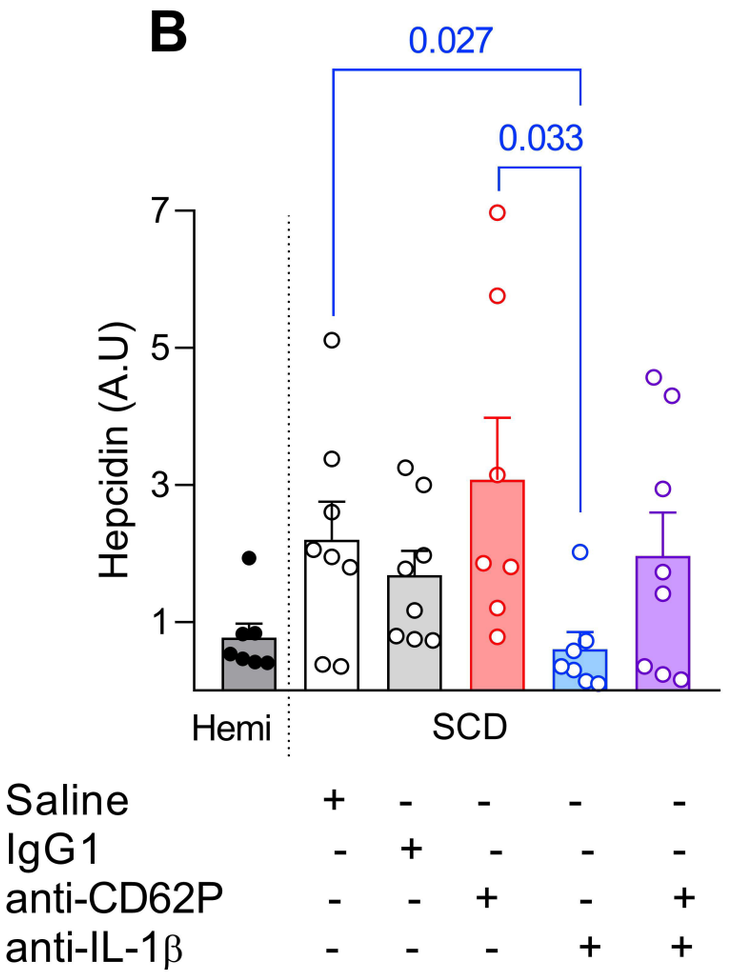
B
0.027
0.033
7
5
3
1
Hepcidin (A.U)
Hemi
SCD
Saline + - - - -
IgG1 - + - - -
anti-CD62P - - + - +
anti-IL-1β - - - + +

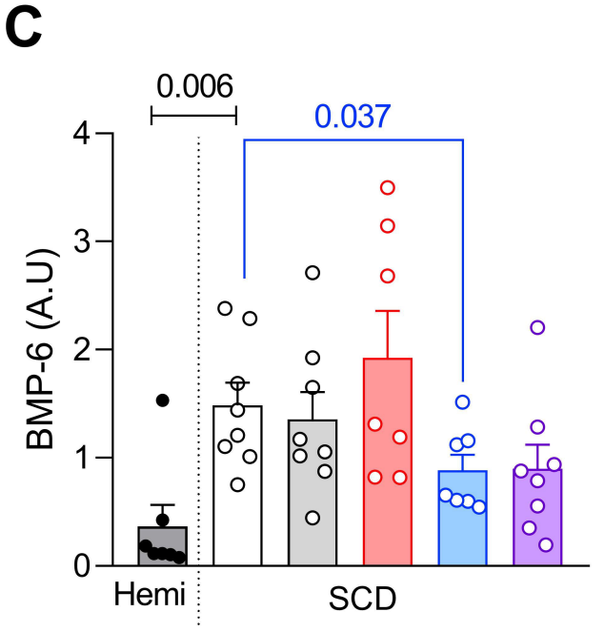
C
0.006
0.037
4
3
2
1
0
BMP-6 (A.U)
Hemi
SCD
Saline + - - - -
IgG1 - + - - -
anti-CD62P - - + - +
anti-IL-1β - - - + +

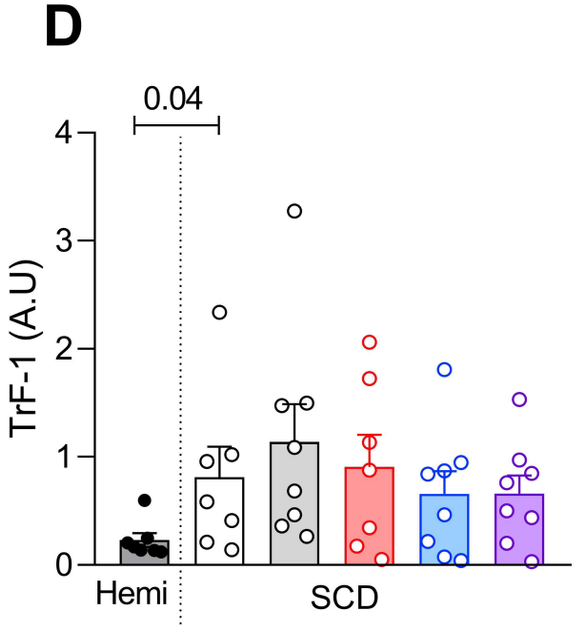
D
0.04
4
3
2
1
0
TrF-1 (A.U)
Hemi
SCD
Saline + - - - -
IgG1 - + - - -
anti-CD62P - - + - +
anti-IL-1β - - - + +

Supplementary Material

Neutralizing P-selectin and interleukin-1β in mice with sickle cell disease: effects on vaso-occlusive processes and organ injury.

Érica M. F. Gotardo, Lidiane S. Torres, Bruna Cunha Zaidan, Lucas F. S. Gushiken, Pâmela L. Brito, Flavia C. Leonardo, Claudia H. Pellizzon, Sergei Agoulnik, Jiri Kovarik, John Millholland, Fernando F. Costa and Nicola Conran

Supplementary Methods

Animals

Male homozygous Townes mice (*B6;129-Hbb$^{tm2(HBG1,HBB*)Tow}$/Hbb$^{tm3(HBG1,HBB)Tow}$ Hba$^{tm1(HBA)Tow}$/J*) and male Berkeley mice (*Hba^{tm1Paz}Hbb^{tm1Tow}Tg(HBA-HBBs*) 41Paz/J) were used in the study.[1,2] Townes mice were used for acute studies to evaluate microvascular vaso-occlusion, based on previous data from our own studies and those of other authors indicating the suitability of this model,[3,4] and the reliability of our breeding supply. For prolonged studies, we used the Berkeley mouse strain, due to literature reports available at the time of study design describing progressive organ damage similar to that of human SCD.[5] Additionally, our preliminary data from this model enabled us to define a suitable starting time of 16 weeks for antibody administration to capture this damage. Mice were bred from breeders purchased originally from The Jackson Laboratories (Maine, EUA) that were maintained by the animal facility (CEMIB) of the University of Campinas. For some analyses, aged-matched hemizygous littermate mice of the Berkeley strain and age-matched C57BL/7J mice were used as controls. After weaning, mice were maintained at Hematology Center Animal House in microisolators until euthanasia, with food and water *ad libitum*.

Treatment Protocols

Acute protocol (see Figure 1A): Eighteen-week old Townes SCD mice received (i.p.) either saline, or anti-murine IL-1β monoclonal antibody (mAb) (01BSUR IgG2a; 200μg/mouse), and/or anti-murine CD62P (RB40.34 IgG1; 30 μg/mouse), or a control IgG1 antibody (A110-1, 30 μg/mouse), before recombinant murine TNF-α (0.5 μg, *i.p.*, R&D Systems, Minnesota, USA) administration to induce VO processes. Analysis of vaso-occlusion and of blood samples was conducted at 3

hours after TNF-α administration. Anti-murine IL-1β or saline were administered at 24 hours before analyses (i.e., 21 hours before TNF-α). Anti-murine CD62P or control IgG1 were administered at 3.5 hours before analyses (i.e., 0.5 hours before TNF-α). These administration times were chosen based on prior studies of the acute administration of each antibody in inflamed murine models of SCD.[6,7] The mechanistic effects of RB40.34 (anti-P-selectin) IgG1 were compared with those of a control IgG1, due to the non-specific effects of this antibody isotype *in vivo*.[8] Conversely, in mice, the IgG2a isotype causes less non-specific immune interference, compared to IgG1.[9] Therefore, the effects of 01BSUR administration were compared to those of saline. Additionally, the effects of the combined antibody administration were compared to those of control IgG1.

Chronic protocol (see Figure 3A): Sixteen-week old Berkeley SCD mice received (i.p.) anti-IL-1β mAb (7.5 mg/Kg; 2x/week), and/or anti-murine CD62P (30 μg/mouse; 3x/week), or an IgG1 mAb (30 μg/mouse; 3x/week) or saline (2x/week) for 6 weeks. At the end of the treatment, and at 48 hours after the last administration of antibodies, the animals were euthanized and their biological materials collected or analyses carried out. Antibody dosing protocols were used to determine the optimal mAb concentrations and frequencies of administration. Optimal dose concentrations and frequencies of prolonged administration were determined using standardizing protocols, namely maintenance of the inhibition of neutrophil-platelet ($CD45^+Ly6G^+CD41^+$) aggregate formation or reduction of serum IL-6 for 2 weeks (for anti-P-selectin or anti-Il-1β, respectively).

Laser Doppler flowmetry

After anesthesia and trichotomy, laser Doppler flowmetry of the skin microcirculation of the pelvic region of immobilized animals was conducted using the PeriFlux6000 equipment (Perimed, Sweden), employing a 780 nm wavelength laser and the 407 probe. Blood perfusion (in perfusion units) in the pelvic skin microcirculation, within a 10-minute period, was calculated from the mean red blood cell concentration and mean red cell flow velocity (velocity units) using the PeriFlux Configuration Software (PCS). Measurements were normalized relative to each animal's baseline blood perfusion and velocity recorded 48 h earlier.

Intravital Microscopy

Mice were anesthetized at 3-h post TNF-α administration by *i.p.* injection of a ketamine 100 mg/kg + xylazine 10 mg/kg mixture in saline. For the surgical procedure, the animal's cremaster muscle was exteriorized, and stretched over a transparent platform, and continuously irrigated with Ringer's solution (pH 7.4, 37°C). Microvessels (5-9 for each mouse) of 25-35 μm in diameter were visualized using an Axio Imager D2 (Carl Zeiss Microscopy, Jena, Germany; 63X water

immersion objective) that was custom-designed for intravital microscopy. Images from vessels were recorded for 30-60 seconds (40 frames/sec) using an Axiocam 506 color camera (Carl Zeiss Microscopy) and the Zen 2 Pro software (Carl Zeiss Microscopy). The rolling, adhesion and extravasation of leukocytes were quantified according to Almeida et al. (2015).[10] Imaging was performed for a maximum period of 45 min after surgery.

Neutrophil-platelet aggregate analysis by flow cytometry.

Briefly, 50 µl of blood were collected from the retro-orbital plexus with a heparinized capillary. Blood was then incubated with a mix of antibodies in Hank's buffer: PerCP anti-mouse CD45 (30-F11, BioLegend, San Diego, CA, USA), APC anti-mouse Ly6G (1A8, BioLegend) and PE anti-mouse CD41 (MWReg30, BD Biosciences). The samples were stained for 30 min in the dark, at room temperature (RT). After labeling, lysis buffer (1 x Lysing Buffer, BD Biosciences) was added and cells were incubated for 15 min in the dark (RT). After centrifugation (200 *g*, 5 min, RT) and washing, the cell pellets were resuspended in PBS/BSA buffer and data acquisition (50,000 events) was performed on a FACSCalibur™ Flow Cytometer (BD Biosciences). Representative dot plots and analysis of the aggregates are shown in Supplementary Figure 1.

Inflammatory and biochemical marker quantification

IL-1β, tumor necrosis factor (TNF)-α, Interferon (INF)-γ, soluble adhesion molecule intercellular adhesion molecule (sICAM)-1 and IL-6 were measured in serum samples using commercial ELISA kits (IL-1β [high-sensitivity], TNF-α [high-sensitivity], INF-γ, sICAM-1; R&D Systems, Minneapolis, MN, USA. IL-6 [high-sensitivity]; Invitrogen, Vienna, Austria), according to the manufacturers' instructions. Aspartate aminotransferase (ALT) and Alanine aminotransferase (AST) liver enzymes and bilirubin (total, direct and indirect) were quantified in serum, while creatinine was quantified in urine collected on the day of euthanasia, using commercial colorimetric tests (Bioclin, Belo Horizonte, MG, Brazil).

Organ processing and histological staining

Organ specimens were dissected, fixed in 10% formalin solution, and dehydrated in an ethanol sequence before embedding in paraffin. Five-µm sections were stained for histology using hematoxylin-eosin or Masson's trichrome. For evaluating hemosiderin accumulation, sections were incubated with potassium ferrocyanide and hydrochloric acid aqueous solution (1:1 ratio), counterstained with Nuclear Fast Red, and the Prussian blue reaction observed. Areas of sections stained with Prussian blue or Masson's trichome were calculated using Image J analysis software (10 fields/section). The histological analysis of 2-4 sections from each organ was performed blinded by a pathologist, and alterations were scored per organ qualitatively on a scale of 0 (absent), 1 (mild), 2 (moderate) and 3 (severe). Another pathologist carried out a

blinded morphometric analysis on liver sections (2 sections/ organ), counting the number of vessels with at least one red blood cell inside. Histopathological scores for hepatic degeneration, necrosis, renal RBC sickling, alveolar congestion, and pulmonary septal thickening represent the means and SEM of the comprehensive evaluations for each organ assessed; other parameters are depicted as means and SEM of parameter observations from two to three sections or regions of interest per organ evaluated.

lmmunohistochemical Staining

Immunohistochemical staining was performed on paraffin-embedded tissues. Following deparaffinization and rehydration, slides were subjected to heat-mediated antigen retrieval with Tris-EDTA buffer (pH 9.0) in a microwave. After incubating with 30% H_20_2 for 30 min at RT to block endogenous peroxidase activity, slides were incubated overnight with rabbit anti-murine CD68 IgG (EPR23917-164; Abcam, Cambridge, UK) at 4°C. After washing, primary antibody binding was detected using a Rabbit-specific horseradish peroxidase/ 3,3'-Diaminobenzidine detection immunohistochemistry kit (Abcam), according to the manufacturer's instructions. The slides were counterstained with hematoxylin and the percentages of positive-staining cells were calculated using Image J analysis software (10 fields/section).

Quantitative PCR (qPCR)

Organs, dissected at the time of euthanasia, were snap-frozen in liquid nitrogen and stored at -80°C until assay. mRNA was extracted from entire organs using Trizol (Invitrogen, Carlsbad, CA, USA) and a reverse transcription kit was used to synthesize cDNA (RevertAid H Minus First Strand cDNA Synthesis, Thermo Scientific, Waltham, MA, USA). Oligonucleotide primers were designed (Primer-Express; Applied Biosystems, Foster City, CA, USA) to amplify cDNA for conserved regions of the genes encoding proteins of interest (for genes of interest and primer sequences, see Supplementary Table 1); primers were synthesized by IDT (Coralville, Iowa, USA). All samples were assayed in a 12-µL volume containing 10 ng cDNA, 6 µL SYBR Green Master Mix PCR (Applied Biosystems) and gene primers, using a StepOne Real Time PCR System (Applied Biosystems). To confirm the accuracy and reproducibility of the real-time PCR, the intra-assay precision was calculated according to the equation: E(−1 / slope). A dissociation protocol was performed after each run to check for non-specific amplification. Two replicas were run on the plate for each sample. Results are expressed as arbitrary units (A.U.) of gene expression, normalized according to the expressions of Actb and Gpdh through the geNorm program.[11]

Statistical Analysis

Data are expressed as means and standard error of N samples. For comparisons between two groups, the Mann-Whitney test was used. For comparisons between three groups or more, data normality was evaluated. Subsequently, either a One-Way Analysis of Variance (ANOVA) test followed by Dunn's multiple-comparison test (for non-parametric samples) or Holm's-Sidak's multiple comparison test (for parametric samples) was employed. A p value ≤0.05 was considered statistically significant.

Supplementary References.

1. Wu LC, Sun CW, Ryan TM, Pawlik KM, Ren J, Townes TM. Correction of sickle cell disease by homologous recombination in embryonic stem cells. Blood. 2006;108(4):1183-8.
2. Paszty C, Brion CM, Manci E, Witkowska HE, Stevens ME, Mohandas N, et al. Transgenic knockout mice with exclusively human sickle hemoglobin and sickle cell disease. Science. 1997;278(5339):876-8.
3. Jasuja R, Suidan G, Hett SP, Desai K, Le KX, Parks E, et al. Rivipansel: A Small Pan-Selectin Antagonist Improves Cerebral Perfusion and Inhibits Leukocyte Adhesion and in Murine Sickle Cell Disease Model. Blood. 2016;128(22).
4. Torres LS, Gotardo EM, Leonardo FC, Brito PL, Förster I, Kovarik J, et al. Neutralization of Inflammasome-Processed Cytokines Reduces Inflammatory Mechanisms and Leukocyte Recruitment in the Vasculature of TNF-α-Stimulated Sickle Cell Disease Mice. Blood. 2021;138.
5. Manci EA, Hillery CA, Bodian CA, Zhang ZG, Lutty GA, Coller BS. Pathology of Berkeley sickle cell mice: similarities and differences with human sickle cell disease. Blood. 2006;107(4):1651-8.
6. Ghosh S, Flage B, Weidert F, Ofori-Acquah SF. P-selectin plays a role in haem-induced acute lung injury in sickle mice. British Journal of Haematology. 2019;186(2):329-33.
7. Kaul DK, Thangaswamy S, Suzuka SM, Fabry ME, Wanderer AA, Gram H. Anti-Interleukin-1β Antibody-Based Therapy Ameliorates Endothelial Activation and Inflammation in Sickle Mice. Blood. 2011;118(21):388-.
8. Jang JE, Hidalgo A, Frenette PS. Intravenous immunoglobulins modulate neutrophil activation and vascular injury through FcgammaRIII and SHP-1. Circ Res. 2012;110(8):1057-66.
9. Nimmerjahn F, Ravetch JV. Fcgamma receptors as regulators of immune responses. Nat Rev Immunol. 2008;8(1):34-47.
10. Almeida CB, Souza LE, Leonardo FC, Costa FT, Werneck CC, Covas DT, et al. Acute hemolytic vascular inflammatory processes are prevented by nitric oxide replacement or a single dose of hydroxyurea. Blood. 2015;126(6):711-20.
11. Vandesompele J, De Preter K, Pattyn F, Poppe B, Van Roy N, De Paepe A, et al. Accurate normalization of real-time quantitative RT-PCR data by geometric averaging of multiple internal control genes. Genome Biol. 2002;3(7):RESEARCH0034.

Supplementary Table 1. Primers for quantitative Real-Time PCR

Gene	Protein encoded	Primer	Primer concentration
Actb - F *Actb - R*	β-Actin	5´- ACTGCCGCATCCTCTTCCT -3´ 5´- GAACCGCTCGTTGCCAATA- 3´	70nM
Gapdh - F *Gapdh-R*	GAPDH	5´- TGCACCACCAACTGCTTA -3´ 5´- GGATGCAGGGATGATGTTA -3	70nM
Col1a1- F *Col1a1- R*	Collagen Type 1	5´-GAGCGGAGAGTACTGGATCG -3´ 5´- GCTTCTTTTCCTTGGGGTTC- 3´	300nM
Col3a1 -F *Col3a1 -R*	Collagen Type 3	5´-GCACAGCAGTCCAACGTAGA- 3´ 5´- TCTCCAAATGGGATCTCTGG -3´	300 nM
Timp-1 -F *Timp-1 -R*	TIMP-1	5´- GCCTGTAGCTGTGCCCCA -3´ 5´- GGAACCCATGAATTTAGCCCTTAT	300nM
Timp-2 -F *Timp-2 -R*	TIMP-2	5´-GGGTCTCGCTGGACGTTG -3´ 5´- GGGTAATGTGCATCTTGCCAT -3´	300nM
Tgfb1– F *Tgfb1 - R*	TGF-β	5´- AAAGAAGTCACCCGCGTGC -3´ 5´- CCCGAATGTCTGACGTATTGAA -3´	300nM
Hif1a -F *Hif1a -R*	HIF-1α	5´-GAAGCACTAGACAAAGTTCACCTG-3´ 5´- TTAGGCTGGGAAAAGTTAGGAGT- 3´	150nM
Icam1 -F *Icam1 -R*	ICAM-1	5´- CAATTTCTCATGCCGCACAG -3´ 5´- AGCTGGAAGATCGAAAGTCCG -3´	70nM
Havcr1 -F *Havcr1 -R*	KIM-1	5´- GCATCTCTAAGCGTGGTTGC - 3´ 5´-TCAGCTCGGGAATGCACAA -3´	150nM
Lcn2 -F *Lcn2 -R*	NGAL/LCN2	5´- TGAAGGAACGTTTCACCCGCTTTG-3´ 5´- ACAGGAAAGATGGAGTGGCAGACA-3´	150nM
Tfrc -F *Tfrc -R*	TFR1	5´-AATGGTTCGTACAGCAGCGGAAG-3´ 5´- CACGAGCGGAATACAGCCACTG-3´	300nM
Hamp -F *Hamp -R*	Hepcidin	5´-CCTATCTCCATCAACAGATG- 3´ 5´- AACAGATACCACACTGGGAA-3´	300nM
Bmp6 – F *Bmp6 - R*	BMP6	5´- ATGGCAGGACTGGATCATTGC -3´ 5´- CCATCACAGTAGTTGGCAGCG-3´	70nM

GAPDH, glyceraldehyde-3-phosphate dehydrogenase; HIF-1α, Hypoxia-Inducible Factor 1α; ICAM-1, Intercellular adhesion molecule-1 (CD54); KIM-1, kidney injury molecule-1; LCN2/NGAL, neutrophil gelatinase-associated lipocalin; TIMP, Tissue inhibitor of metalloproteinases; TGF-β, Transforming Growth Factor-β.

Supplementary Table 2. Biochemical markers of organ damage in hemi- and homozygous SCD Berkeley mice treated or not with anti-CD62P and/ or anti-IL-1β therapy for 6 weeks

	N	AST (U/ML)[a]	ALT (U/ML)[a]	Total Bilirubin (mg/dL)[a]	Direct Bilirubin (mg/dL)[a]	Indirect Bilirubin (mg/dL)[a]	Creatinine (mg/dL)[b]
Hemizygous control	5	52.3±12.8	9.4±2.2	0.50±0.06	0.13±0.04	0.40±0.5	34.1±2.6
Homozygous SCD							
Saline	8	53.0±9.7	61.1±11.8 ###	1.30±0.2 ##	0.51±0.1 ###	0.92±0.09#	29.0±4.7
IgG1	8	53.5±6.2	68.8±14.5 ###	1.4±0.1 ##	0.52±0.1 ###	0.84±0.08#	24.2±2.3 #
Treatment							
Anti-CD62P	8	53.8±21.8	76.5±17.5	1.5±0.1	0.58±0.1	0.89±0.06	32.4±4.0
Anti-IL-1β	6	50.1±4.9	50.5±9.5	1.3±0.1	0.47±0.1	0.81±0.06	28.9±3.0
Anti-CD62P + anti-IL-1β	7	64.6±5.6	121.5±24.4$	1.5±0.1	0.40±0.06	1.10±0.09*$	31.5±9.9

[a] serum samples and [b] urine samples

Biochemical markers in the serum or urine of aged-matched hemizygous (SA) mice and homozygous (SS) Berkeley mice. Mice (4-months old) received administrations of *i.p.* saline (twice weekly) or *i.p.* injections of 30 µg/mouse IgG1 (three times a week) for six weeks, or were treated with i.p. injections of 30 µg/mouse anti-CD62P (three times a week), and /or 7.5 mg/Kg (twice a week) of anti-IL1β antibody for 6 weeks. Peripheral blood was obtained from animals at 48 hours after the last administration, before animal euthanasia. AST, aspartate aminotransferase; ALT, alanine aminotransferase. #, P<0.05; ##, p<0.01; ###, P<0.001 when compared to hemizygous (SA) mice. *, P<0.05 when compared to IgG1-control SS mice. $, P<0.05 when compared to Anti-IL-1β-treated SS mice.

Supplementary Table 3. Summary of the effects of mono- and combined immunotherapies.

	Vaso-occlusive Processes	Leukocyte-platelet aggregates		Leukocyte rolling	Leukocyte Adhesion	Inflammatory Markers	Biochemical markers	Liver injury	Liver vessel congestion	Liver macrophages	Iron deposition (liver/Kidney)
Anti-P-selectin	↓↓	↓↓	↓↓	↓↓	→	→ →	→	→	→	↓	→
Anti-IL-1β	↓↓	→	→	↓↓	↓↓	sICAM-1↓↓ TNF↓ IL-10 ↓↓ IL-6↓	→	↓↓	↓	↓↓	↓↓
Anti-P-selectin + Anti-IL-1β	↓↓	↓↓	↓↓	↓↓	↓↓	TNF↓	↑ALT, IB	↑*	↓	↓	↓↓

Acute administration effects; Long-term administration effects; → no significant effect; ↓ decrease ($p<0.05$); ↓↓ decrease ($p<0.01$); ↑ increase.

* Histopathological features. ALT, alanine aminotransferase; IB, indirect bilirubin

Supplementary Figures

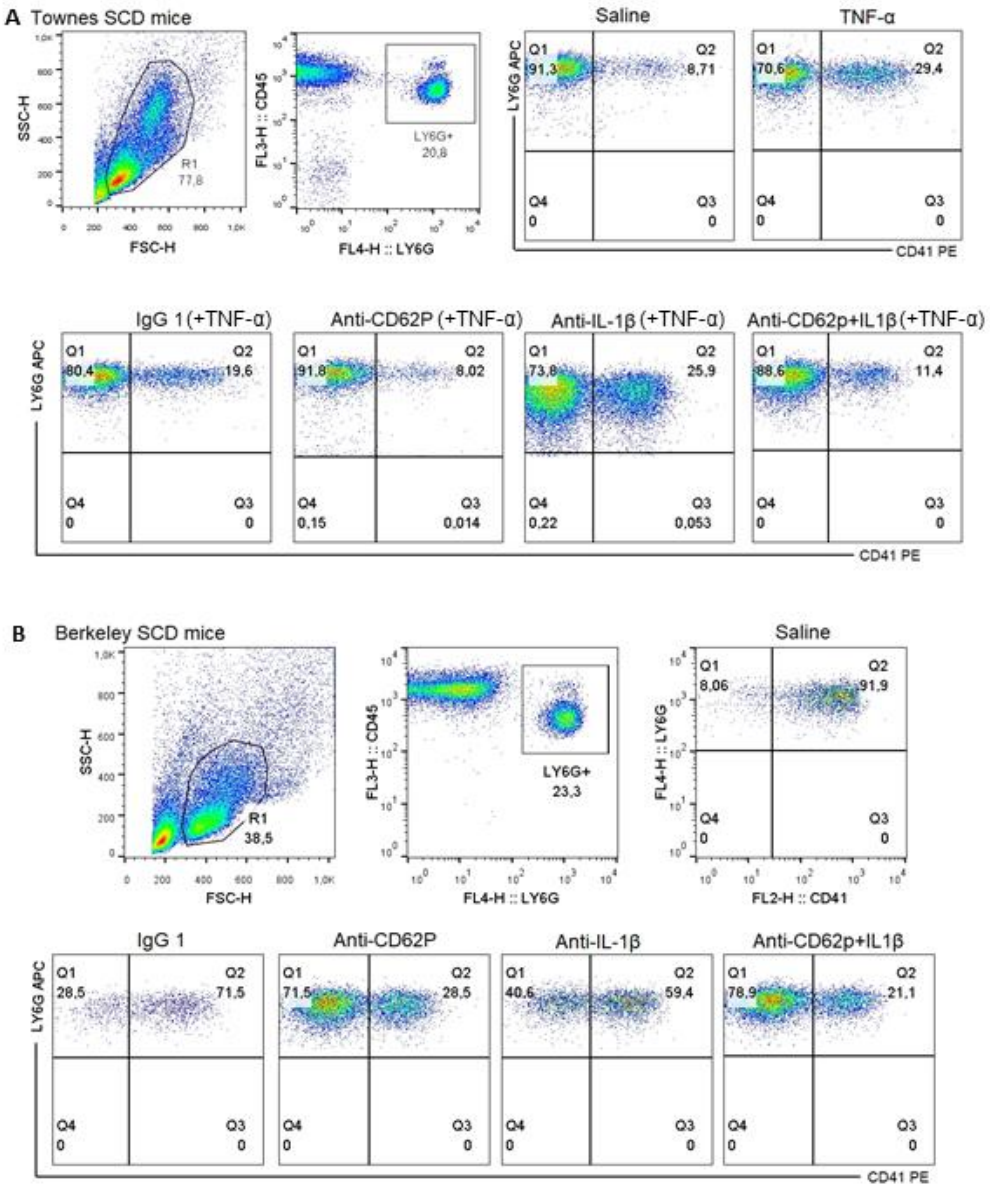

Supplementary Figure 1. Flow cytometry-gating strategy for analysis, and representative dot plots, for neutrophil-platelet aggregates in blood samples from **(A)** Townes mice, and **(B)** Berkeley mice. Peripheral blood was obtained from the retro-orbital plexus of mice and incubated with PerCP anti-mouse CD45, APC anti-mouse Ly6G, and PE anti-mouse CD41, before lysing red blood cells. Data acquisition (50,000 events) was performed on a FACSCalibur™ Flow Cytometer. $CD45^{+}Ly6G^{+}$ neutrophils were gated, and those that also labelled positive for CD41 were considered to be neutrophil-platelet aggregates (calculated using FlowJo V10 analysis software).

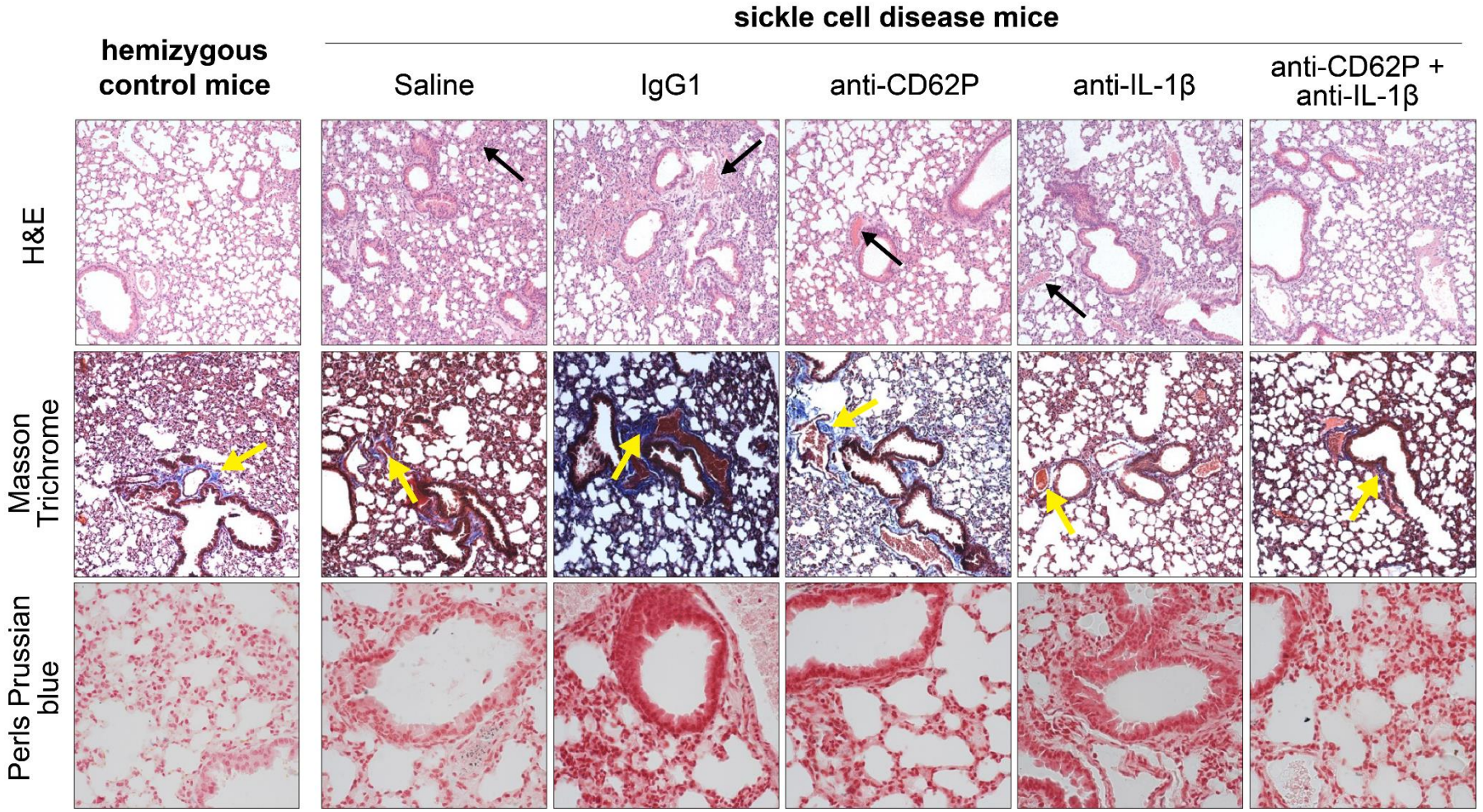

Supplementary Figure 2: Effects of 6-weeks administration of anti-CD62P and anti-IL-1β immunotherapies on lung histology, injury, and iron accumulation in sickle cell disease mice. Berkeley SCD mice (4-months old) were treated, or not, with immunotherapies for 6 weeks. At 48 h after administration of the final intervention dose, lungs were dissected and processed for histological analysis (H & E staining, 20x magnification), analysis of fibrosis (Masson Trichrome, 20x mag.), iron accumulation (Perls Prussian blue, 63x mag.). Representative photographs of stained paraffin-embedded sections from each treatment group and comparison with lung sections from hemizygous Berkeley control mice of the same age. Photographs are representative of four images per section (2-4 sections/mouse). Black arrows: congested vessels; yellow arrows: collagen deposits. Photomicrographs taken with a Zeiss Axio Imager D2.

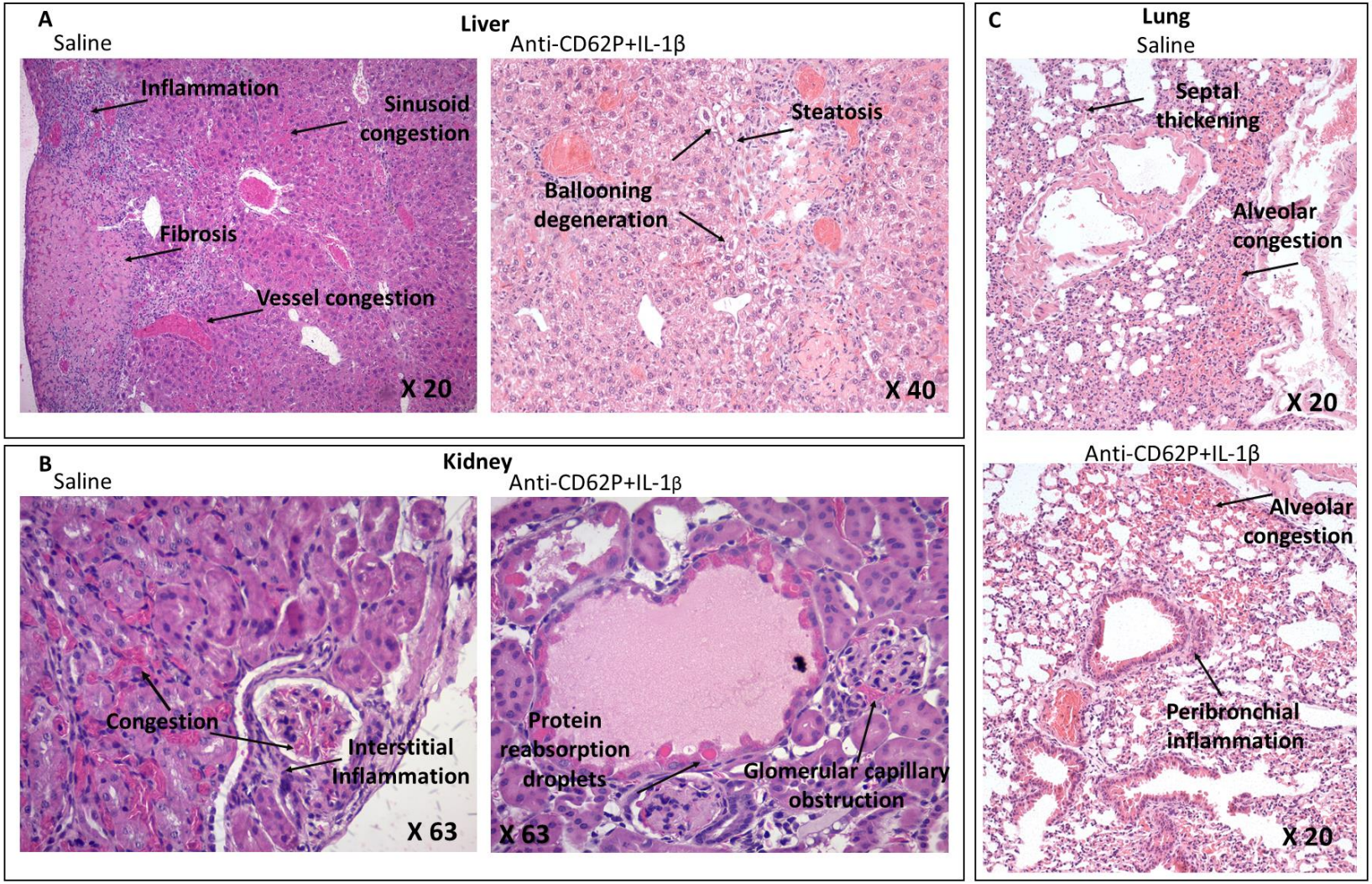

Supplementary Figure 3: Representative histopathological features (H&E staining) observed in the (A) liver, (B) kidney and (C) lung of SCD mice following 6 weeks of administration of saline, or of anti-CD62P and anti-IL-1β combined therapy. Photomicrographs taken with a Nikon microscope, model BM2100.

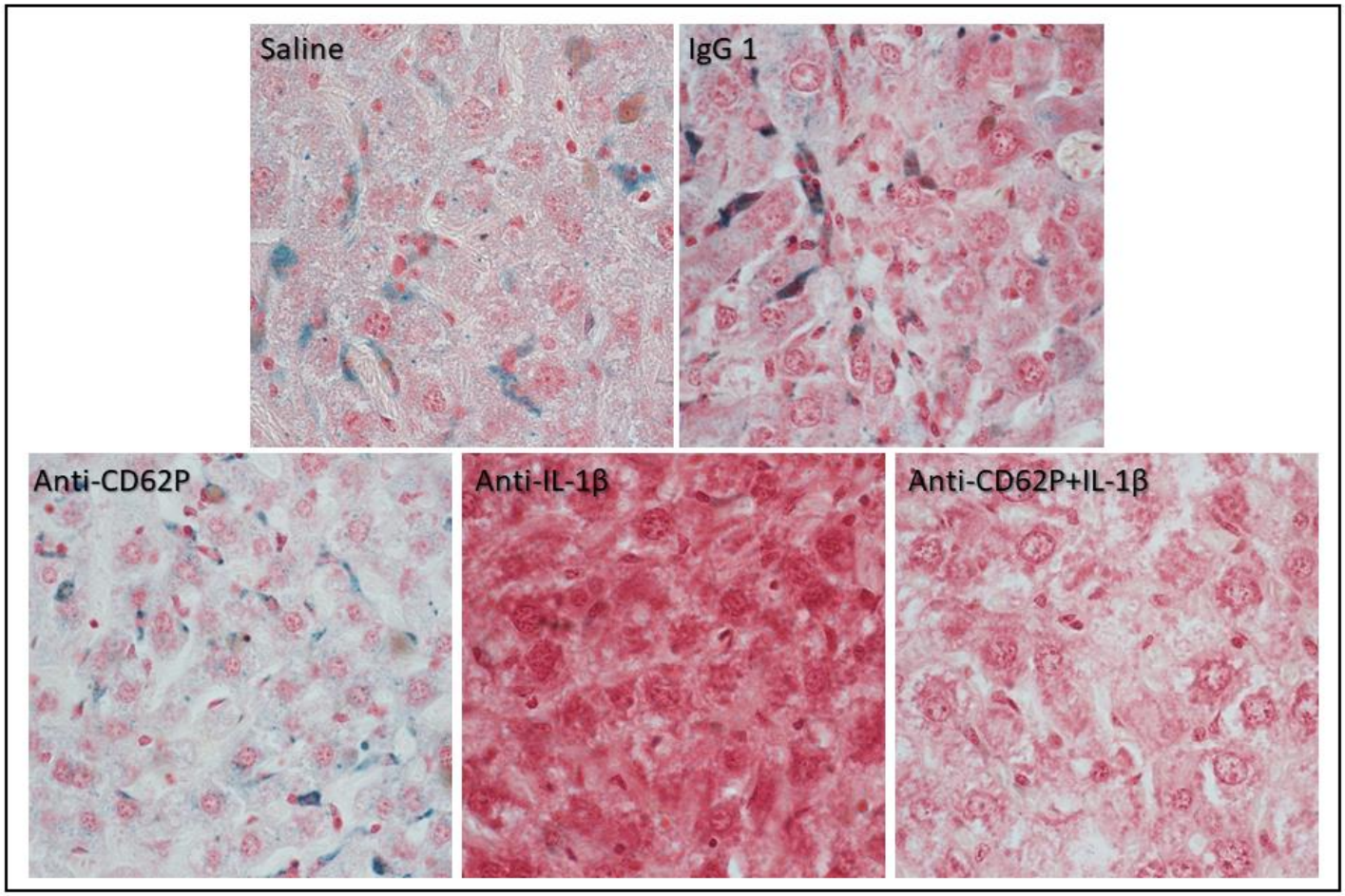

Supplementary Figure 4. Representative high magnification photomicrographs of iron deposition (blue staining) associated with macrophage infiltration in liver sections of Berkeley SCD mice (22 weeks old) after 6 weeks of the indicated administration. Perls staining; livers from anti-IL-1β and anti-CD62P + IL-1β-treated mice did not present iron deposition. Images (X100) were taken with a Zeiss Axio Imager D2.

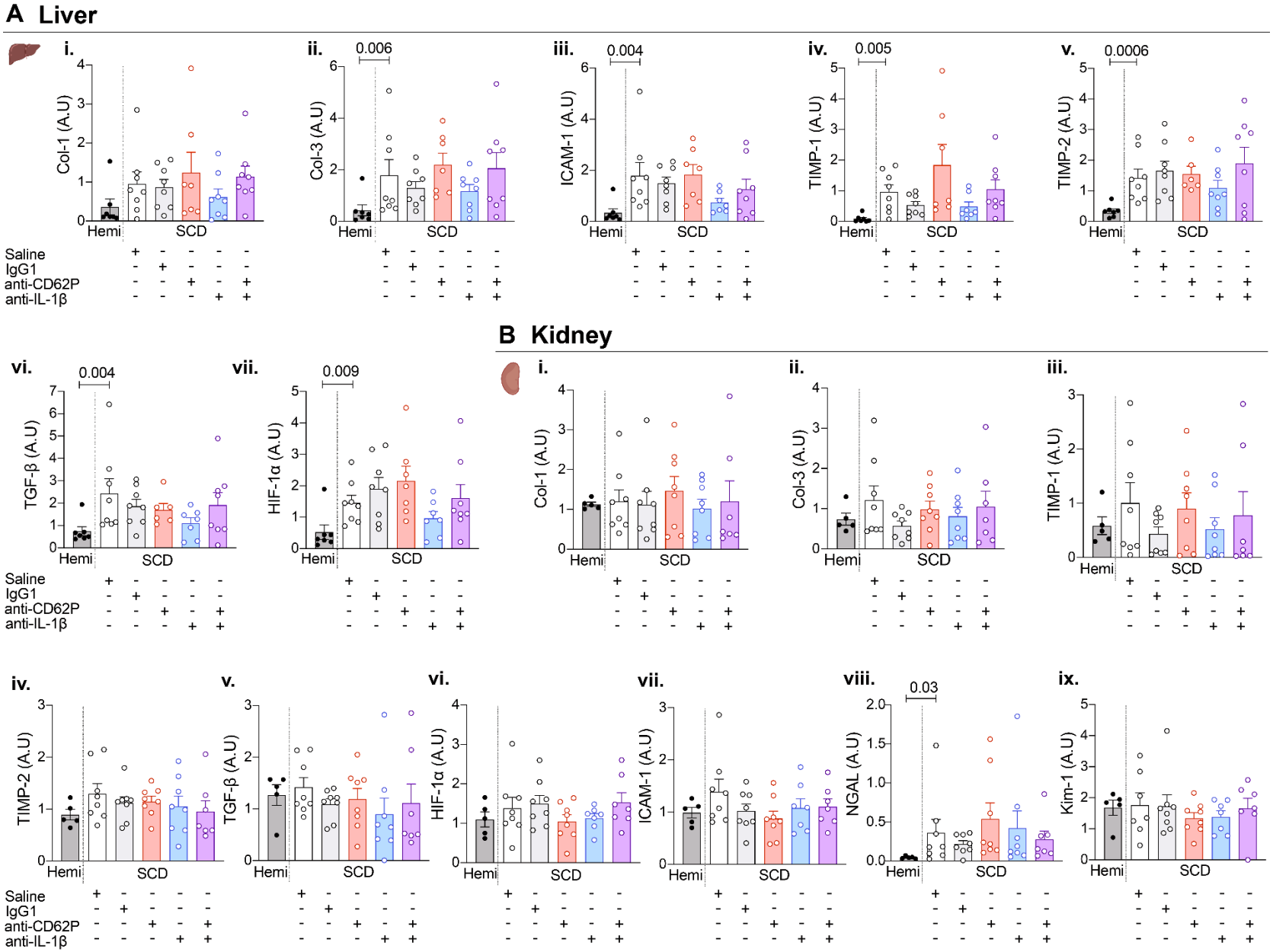

Supplementary Figure 5. Gene expressions of biomarkers of inflammation and damage in organs of aged-matched hemizygous and homozygous Berkeley SCD mice following treatment for 6 weeks, according to Figure 3A. (A) Liver, and (B) kidney. Genes and their encoded proteins are described in the Supplementary Table 1; expressions were quantified by qPCR.